IEEE Journal of Selected Topics in Applied Earth Observations and Remote Sensing

Simultaneous Estimation of Sub-canopy Topography and Forest Height with Single-baseline Single-polarization TanDEM-X Interferometric Data Combined with ICESat-2 Data

Zhiwei Liu, Jianjun Zhu, Juan M. Lopez-Sanchez, *Senior Member, IEEE*, Cristina Gómez, Haiqiang Fu, *Senior Member, IEEE*, Cui Zhou, Huiqiang Wang, and Rong Zhao

***Abstract*—To address the challenge of retrieving sub-canopy topography using single-baseline single-polarization TanDEM-X InSAR data, we propose a novel InSAR processing framework. Our methodology begins by employing the SINC model to estimate the penetration depth (PD). Subsequently, we establish a linear relationship between PD and phase center height (PCH) to generate a wall-to-wall PCH product. To achieve this, space-borne LiDAR data are employed to capture the elevation bias between actual ground elevation and InSAR-derived elevation. Finally, the sub-canopy topography is derived by subtracting the PCH from the conventional InSAR-based DEM. Moreover, this approach enables the simultaneous estimation of forest height from single-baseline TanDEM-X data by combining the estimated PD and PCH components. The approach has been validated against Airborne Lidar Scanning data over four diverse sites encompassing different forest types, terrain conditions, and climates. The derived sub-canopy topography in the boreal and hemi-boreal forest sites (Krycklan and Remningstorp) demonstrated notable improvement in accuracy. Additionally, the winter acquisitions outperformed the summer ones in terms of inversion accuracy. The achieved RMSEs for the winter scenarios were 2.45 m and 3.83 m, respectively, representing a 50% improvement over the InSAR-based DEMs. And the forest heights are also close to the ALS measurements, with RMSEs of 2.70 m and 3.33 m, respectively. For the Yanguas site in Spain, characterized by rugged terrain, sub-canopy topography in forest areas was estimated with an accuracy of 4.27m, a 35% improvement over the original DEM. For the denser tropical forest site, only an average elevation bias could be corrected.**

***Index Terms*—Interferometric synthetic aperture radar (InSAR), TanDEM-X, ICESat-2, forest, sub-canopy topography.**

I. Introduction

DIGITAL Terrain Models (DTMs) are crucial datasets for applications such as forest management planning, flood delineation, and hazard monitoring [1], [2], [3], [4], among others. Currently, three remote sensing techniques, namely optical photogrammetry, light detection and ranging (LiDAR), and interferometric synthetic aperture radar (InSAR), are extensively employed to generate Digital Elevation Models (DEMs) on both local and global scale. For instance, widely recognized DEMs, such as SRTM DEM and ASTER GDEM, have been produced using these techniques.

In forested areas, capturing the topography beneath the vegetation is a persistent challenge, and the DEMs generated thereby very seldom meet the accuracy requirements of the above-mentioned applications. For instance, optical photogrammetry alone can only provide the elevation of the canopy surface, necessitating auxiliary data to estimate the sub-canopy topography [5]. While LiDAR has the ability to detect sub-canopy topography, it is typically unsuitable for wall-to-wall topographic mapping at global scale when concerning space-borne LiDAR platforms. In reference to airborne LiDAR systems, although they have ability to deliver fine spatial resolution data for topography and forest height retrieval, their current availability is limited to a few developed countries due

This work is funded by the National Key R&D Program of China (No. 2022YFB3902605), the National Natural Science Foundation of China (Nos. 42227801, 42030112, 42204024, 42104016, 42330717), the Spanish Ministry of Science and Innovation (State Agency of Research, AEI) and the European Funds for Regional Development under Project PID2020-117303GB-C22/AEI/10.13039/501100011033, the Natural Science Foundation for Excellent Young Scholars of Hunan Province (No. 2023JJ20061), and in part by the China Scholarship Council Foundation to the Joint Ph.D. Studies at University of Alicante (No. 202106370125). (*Corresponding author: Jian Jun Zhu*).

Zhiwei Liu is with the School of Geoscience and Info-Physics, Central South University, 410083 Changsha, China, and also with the Institute for Computer Research (IUII), University of Alicante, 03080 Alicante, Spain (e-mail: liuzhiwei@csu.edu.cn).

Jianjun Zhu and Haiqiang Fu are with the School of Geoscience and Info-Physics, Central South University, 410083 Changsha, China (e-mail: zjj@csu.edu.cn, haiqiangfu@csu.edu.cn).

Juan M. Lopez-Sanchez is with the Institute for Computer Research (IUII), University of Alicante, 03080 Alicante, Spain (e-mail: juanma-lopez@ieee.org).

Cristina Gómez is with the iuFOR-EiFAB Campus de Soria, University of Valladolid, 42004 Soria, Spain, and also with the University of Aberdeen, Aberdeen, AB24 3UE, Scotland, U.K. (e-mail: cgomez@uva.es).

Cui Zhou is with the College of Advanced Interdisciplinary Studies, Central South University of Forestry and Technology, 410004 Changsha, China (e-mail: cuizhou@csuft.edu.cn).

Huiqiang Wang is with the College of Water Conservancy and Civil Engineering, Inner Mongolia Agricultural University, 010018 Hohhot, China (e-mail: huiqiangwang@imau.edu.cn).

Rong Zhao is with the College of Advanced Interdisciplinary Studies, Central South University of Forestry and Technology, 410004 Changsha, China (e-mail: zhaorong1018@126.com).

to the high cost and the difficulty associated with processing huge datasets. In the case of InSAR, which utilizes microwaves and can penetrate the canopy layer, the measured elevation is typically situated between the top of the canopy and the ground surface [6], as indicated by the blue curve in Fig. 1. Nonetheless, InSAR is regarded as a potential tool for measuring forest height and sub-canopy topography since not only measures height but also captures the vertical structure of the forest. Note that the term "InSAR" in this context specifically refers to data acquisition conducted under the single-baseline single-polarization mode.

The primary limitation of InSAR data for simultaneous sub-canopy topography and forest height inversion stems from the insufficient number of observations it provides (only one complex coherence, i.e., two real values), which makes it challenging to directly distinguish between the ground and the canopy in the received radar signal [7]. To address this challenge, various algorithms have been developed to enhance the number of observations, such as utilizing multi-polarization [8], multi-frequency [9], multi-squint–angle (sub-aperture) InSAR [10], dual/multi-baseline [11], [12], or tomographic SAR configurations [13], [14]. In the realm of these techniques, the most commonly utilized method for simultaneous forest height inversion and sub-canopy topography mapping is polarimetric InSAR (PolInSAR). However, most space-borne systems operate in repeat-pass interferometric mode, and, consequently, the presence of temporal decorrelation significantly degrades the quality of the interferograms, thereby constraining the effectiveness of PolInSAR inversion [15], [16].

TanDEM-X emerged as a noteworthy single-pass space-borne polarimetric SAR interferometer, which has acquired global single-polarization interferometric data and also dual/quad-polarimetric experimental data in local regions, without temporal decorrelation [17]. Previous studies have demonstrated the feasibility of inverting forest height using dual-polarimetric [16] and quad-polarimetric TanDEM-X PolInSAR data [18]. However, to achieve global applicability, it is important to note that the standard acquisition mode of TanDEM-X constellation is in single-polarization. This limitation restricts the application of PolInSAR inversion approaches due to the insufficient coverage.

Regarding single-polarization TanDEM-X InSAR data, several algorithms have been proposed for forest canopy height inversion by incorporating an external ground elevation model (i.e., DTM) [19], [20], [21], [22], [23]. However, these methods can only be applied in areas where a DTM is available, and, by definition, they cannot be used for extracting sub-canopy topography. To reduce the reliance on external DTMs, other methods employ simplified scattering models to establish a relationship between the observed coherence and forest parameters (canopy height and density), for instance, the SINC-model [24] and its variants [25], [26], as well as the two-level model (TLM) [6], [27]. More recently, the direct use of LiDAR waveforms to define the vertical reflectivity profile has been proposed [28], [29]. In these manners, the forest canopy height can be inversed based solely on single-baseline single-polarization InSAR data. Still, they do not directly enable the extraction of sub-canopy topography.

When it comes to estimating sub-canopy topography using TanDEM-X InSAR data, the main typical step consists in estimating the phase center height (PCH) produced by the forest volume scattering and then removing it from the conventional InSAR-based DEM. To this aim, a dual-baseline TLM inversion approach was proposed and demonstrated in [11]. However, this method requires the SAR to be acquired in alternating bistatic cooperative mode, in order to create dual-baseline combination that are acquired near-simultaneously. To meet the requirements of conventional bistatic InSAR acquisitions, an approach based on interferometry was developed and validated in [30]. However, it requires that the radar signals penetrate through the forest layer and measure a significant ground-scattering contribution [12]. Furthermore, its effectiveness is notably influenced by the terrain slope. To address this issue, the study in [31] proposed a composite model to extract sub-canopy topography. For this purpose, a linear relationship between the penetration depth (PD), estimated based on an infinitely deep penetration model [32], and reference forest height data (from external LiDAR acquisitions) was established to later estimate a wall-to-wall PCH map. However, this approach assumes that forest scenes consist of infinitely deep uniform volumes, which is not true in the majority of cases. In addition, it has to cope with potential measurement bias between SAR and LiDAR forest height data, caused by the time gap between acquisitions and natural vegetation growth.

Following this line of research, the first goal of this paper is to present a novel InSAR processing framework for enhancing the mapping of sub-canopy topography using single-baseline single-polarization TanDEM-X InSAR data. The core idea behind our approach involves the separation of the PCH from the total interferometric phase. To accomplish this objective, we utilize the SINC-model to characterize the scattering behavior of X-band microwaves in forested areas, resulting in the PD, which represents the height difference from the top of the canopy to the average phase center. Subsequently, based on the linear relationship between forest height and either PCH [21], [22], [23] or PD [24], [25], [26], the PD is employed as a surrogate for the estimation of wall-to-wall PCH by a linear function model (section II.B). In such way, we establish a reliable sub-canopy topography estimation method (section II.C). Furthermore, as a second goal, our approach is also utilized to generate forest canopy height estimates by combining the estimated PCH and PD components.

In order to support the solution of the proposed model, the availability of ground points is essential. For this purpose, in this study we utilize ground height measurements obtained from the ICESat-2 mission. The rationale for selecting ICESat-2 data for this study stems from its extensive coverage of Earth's land surface. Among current space-borne LiDAR missions, ICESat-2 spans the widest range of latitudes, from 88º S to 88º N, which allows us to explore and evaluate the proposed approach on a larger geographical scale. Having said this, it is

important to note that the proposed approach does not impose any constraints on the source of the ground reference data used.

In summary, this work constitutes the first attempt in the literature to integrate a scattering model into the radar altimetry model for *simultaneous* retrieval of sub-canopy topography and canopy height *based on single-baseline single-polarization InSAR data*. The main contributions of this work are summarized in the next points:

- The proposed method enables simultaneous retrieval of both sub-canopy topography and canopy height from single-baseline single-polarization TanDEM-X InSAR data.
- A novel data processing framework for fusing acquisitions from different sensors is provided.
- The utilization of sparse ICESat-2 ground data overcomes the limitations arising from the time gap between different sensors and helps calibrate systematic errors associated with imprecise orbital parameters.
- The effects of forest seasonality, forest type, and terrain are assessed over four different test sites.

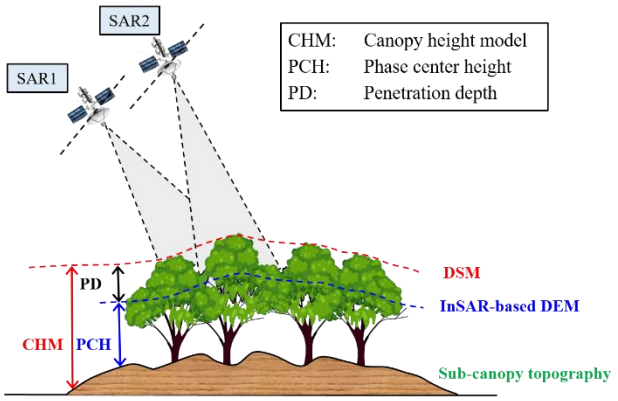

Fig. 1. Schematic representation of sub-canopy topography estimation.

II. Methodology

For two SAR images s_1 and s_2, the complex interferometric coherence can be expressed as

$$\gamma = \frac{E[s_1 \cdot s_2^*]}{\sqrt{E[|s_1|^2]}\sqrt{E[|s_2|^2]}} \quad (1)$$

where $E[\bullet]$ denotes the expectation value operator, and $*$ stands for the complex conjugate operator. The measurement of γ contains both phase and coherence magnitude information, which can be used for different purposes, such as measuring topography from the phase information [33], [34], [35], estimating 3-D vegetation parameters using the coherence amplitude information [6], [19], [24]. Based on both the phase and coherence amplitude measurements, we present a method for the simultaneous estimation of sub-canopy topography and forest canopy height.

A. Phase Components of the TanDEM-X InSAR data

A single-pass (or bistatic) TanDEM-X InSAR pair is acquired by one satellite transmitting radar pulses while both satellites receiving simultaneously the radar echoes from the illuminated targets. In forested area, the complex interferometric coherence shown in (1) can be factorized as [36], [37],

$$\gamma = e^{i\phi_{SCT}} \gamma_{Range} \gamma_{Azimuth} \gamma_{Quant} \gamma_{SNR} \gamma_{Vol} \quad (2)$$

where ϕ_{SCT} represents the phase related to the ground surface height, while the other terms represent decorrelation due to: spatial baseline (γ_{Range}), relative shift of Doppler spectra ($\gamma_{Azimuth}$), quantization errors (γ_{Quant}), limited signal-to-noise ratio (γ_{SNR}), and volume decorrelation (γ_{Vol}) linked to the vertical profile characteristics of the vegetation layer. To isolate γ_{Vol}, γ_{Range} and $\gamma_{Azimuth}$ can be reduced or removed using the range and azimuth spectral filtering, while γ_{Quant} can be compensated by assuming a constant decorrelation influence, such as $\gamma_{Quant} = 0.965$ in this study. Furthermore, γ_{SNR} can also be compensated according to the SAR system parameter using the method given in [16]. Therefore, the volume decorrelation γ_{Vol} stands as the only remaining contribution to decorrelation, and (2) can further be rewritten as,

$$\arg(\gamma) = \arg\left(e^{i\phi_{SCT}}\right) + \arg(\gamma_{Vol}) \quad (3)$$

Since X-band waves can penetrate the forest canopy layer to some extent, the derived InSAR-based DEM (indicated by the blue curve in Fig. 1) is typically located at a certain height below the top of the canopy and represents a DEM between the actual digital surface model (DSM) and the actual DTM. Furthermore, by means of the current InSAR techniques the topographic phase component cannot be separated from the total interferometric phase using only phase information. Therefore, it becomes necessary to seek additional information contained in the InSAR measurements for the sub-canopy topography extraction.

B. Phase Center Height Estimation from Coherence Amplitude

Another key InSAR observable is the interferometric coherence amplitude, which depends on several decorrelation factors, as shown in (2). After compensating for all system-induced decorrelation contributions, the volume decorrelation ($\tilde{\gamma}_{Vol}$) can be modelled by employing a scene model, such as random volume over ground (RVoG) model [38], two-level model (TLM) [6], and interferometric water cloud model (IWCM) [39], each of which is proposed and established based on different physical assumptions [27]. However, due to the complex nature of these theoretical coherence models, the inversion typically necessitates fully-polarimetric acquisitions under the single-baseline condition. Therefore, to force a balanced inversion problem from a single-baseline TanDEM-X InSAR data, simplifications were suggested [6], [8], [16], [26].

Under the RVoG model framework [38], [40], volume decorrelation after compensating for all system-induced decorrelation contributions can be written as,

$$\tilde{\gamma}_{Vol} = e^{i\phi_{SCT}} \frac{\int_0^{h_V} f(z) e^{ik_z z} dz}{\int_0^{h_V} f(z) dz} \quad (4)$$

where h_V is the top height of the forest volume, $f(z)$ is the radar reflectivity function (also named the vertical reflectivity profile), k_z is the vertical wavenumber that depends on the slant

range R, perpendicular baseline $B_\perp$, radar wavelength λ, and local incidence angle θ, as

$$k_z = \frac{2\pi B_\perp}{\lambda R \sin\theta} \quad (5)$$

In (4), there is only one complex measurement $\tilde{\gamma}_{Vol}$ and three real unknown parameters (ϕ_{SCT}, $f(z)$, h_v). In the absence of a precise DTM, only the coherence amplitude can be used for retrieval. Thus, (4) can be rewritten as,

$$|\tilde{\gamma}_{Vol}| = \left| \frac{\int_0^{h_V} f(z) e^{ik_z z} dz}{\int_0^{h_V} f(z) dz} \right| \quad (6)$$

In this manner, (6) can be inverted for forest height h_V using a known or assumed the vertical reflectivity profile $f(z)$. To achieve this, some prior studies have suggested utilizing LiDAR waveforms as the vertical reflectivity function $f(z)$ in (6) to estimate the forest height [28], [29]. To simplify the inversion procedure, we assume $f(z) = 1$, representing a special constant structure function. In this case, the scene is composed of only a homogeneous layer of thickness h_V volume (i.e., forest canopy height), and scattering is uniform (constant) from all the positions in the layer, and (6) can be expressed by a SINC function [39], [41], as,

$$|\tilde{\gamma}_{Vol}| = |\mathrm{sinc}(k_z h_V/2)| \quad (7)$$

By assuming a uniform structure function for medium, (7) implies that the phase center lies around half the actual vegetation volume height h_V. In practical scenarios, extinction affects propagation scattering, so the effective depth producing volume decorrelation is not simply half of the actual top height, but rather a function of it. Therefore, (7) can be inverted with an approximate analytical expression [39] to estimate h_V from the volume coherence amplitude:

$$h_V = k \cdot \frac{1}{k_z}(\pi - 2\sin^{-1}(|\tilde{\gamma}_{Vol}|^{0.8})) \quad (8)$$

where k is a scaling factor to adjust the inversion function according to the specific forest scenario. Essentially, the second term of (8) signifies the effective penetration depth (PD) of microwave signals [39], which can be expressed by,

$$h_{pd} = \frac{1}{k_z}(\pi - 2\sin^{-1}(|\tilde{\gamma}_{Vol}|^{0.8})) \quad (9)$$

In addition, as in previous studies [21], [22], [23], there exists a linear relationship between the forest height and PCH (h_{pch}), so h_{pch} can be expressed in terms of the PD (h_{pd}), as

$$h_{pch} = K \cdot h_{pd} + q \quad (10)$$

where K and q are fitting parameters to establish such a linear relationship.

A notable benefit of (9-10) is its applicability for PCH estimation using coherence magnitude alone. Regarding its performance, on the one hand, it relies on the sensitivity of the chosen baseline. As shown in [24], it is recommended to choose a baseline with a height of ambiguity (HoA: $hoa = 2\pi/k_z$) in the range two to four times the forest height. This choice maximizes the sensitivity and minimizes ambiguity issues during the forest height inversion. However, it is important to emphasize that the accuracy of topography inversion with InSAR is directly proportional to the perpendicular baseline (i.e., k_z). Therefore, achieving a delicate balance between these two factors is crucial for the baseline selection. On the other hand, its performance depends on the forest scenario due to the assumptions considered, i.e., the forest vegetation is a randomly oriented medium with null signal extinction, and the ground is barely visible on the radar echoes (null ground scattering contribution). Fortunately, this issue can be alleviated by the scaling factor K, which allows us to adaptively adjust this model in accordance with the specific forest scenarios.

C. Sub-canopy Topography Estimation Model

By incorporating (9-10) into the conventional phase-to-height conversion model, a sub-canopy topography estimation model can be derived as,

$$h_{sub\_canopy} = \frac{1}{k_z} \cdot \varphi - K \cdot \frac{1}{k_z}(\pi - 2\sin^{-1}(|\tilde{\gamma}_{Vol}|^{0.8})) - q \quad (11)$$

where φ is the unwrapped topographic phase, and q expresses the overall elevation offset between the real sub-canopy topography and the estimated value. In such a way, the sub-canopy topography can be estimated using the interferometric phase and coherence amplitude from single-baseline InSAR measurement. However, before estimating the sub-canopy topography for the entire SAR scene via (11), some ground data need to be provided to determine the unknown parameters K and q. To achieve this goal, we utilize the iterated weighted least-square (IWLS) method with some ICESat-2 ground elevation points. The initial parameters are estimated by

$$\hat{X} = (B^T P B)^{-1}(B^T P L) \quad (12)$$

where $B = \begin{pmatrix} -\frac{1}{k_z^1}(\pi - 2\sin^{-1}(|\tilde{\gamma}_{Vol}^1|^{0.8}) & -1 \\ -\frac{\pi}{k_z^2}(\pi - 2\sin^{-1}(|\tilde{\gamma}_{Vol}^2|^{0.8}) & -1 \\ \vdots & \vdots \\ -\frac{1}{k_z^n}(\pi - 2\sin^{-1}(|\tilde{\gamma}_{Vol}^n|^{0.8}) & -1 \end{pmatrix}$,

$L = \begin{pmatrix} h_1 - \frac{\varphi_1}{k_z^1} \\ h_2 - \frac{\varphi_2}{k_z^2} \\ \vdots \\ h_n - \frac{\varphi_n}{k_z^n} \end{pmatrix}$, $\hat{X} = \begin{pmatrix} K \\ q \end{pmatrix}$,

and h_i $(i = 1,2,\cdots,n)$ represent the terrain elevation at each LiDAR footprint, φ_i $(i = 1,2,\cdots,n)$ correspond to the unwrapped phases, and P denotes an $n \times n$ diagonal weight matrix. Subsequently, the weighted regression can be iterated by placing weights on the observations depending on their associated error or variance [42]. Once the unknown parameters in (11) were determined, we can calculate the PCH value over every pixel with the associated coherence magnitude by

$$h_{pch}^i = K \cdot \frac{1}{k_z^i}\left(\pi - 2\sin^{-1}\left(|\tilde{\gamma}_{Vol}^i|^{0.8}\right)\right) + q \quad (13)$$

Finally, the sub-canopy topography can be derived by subtracting the estimated PCH from the conventional InSAR-based DEM. Meanwhile, by combining the resulting PCH and the estimated PD components, we can also generate the total forest canopy height product.

It is important to note that, for bare surfaces or low vegetation areas, the InSAR phase center should be close to 0, but in these cases the proposed method may result in an underestimated ground elevation due to the inevitable loss of coherence. To address this issue, we set a coherence threshold

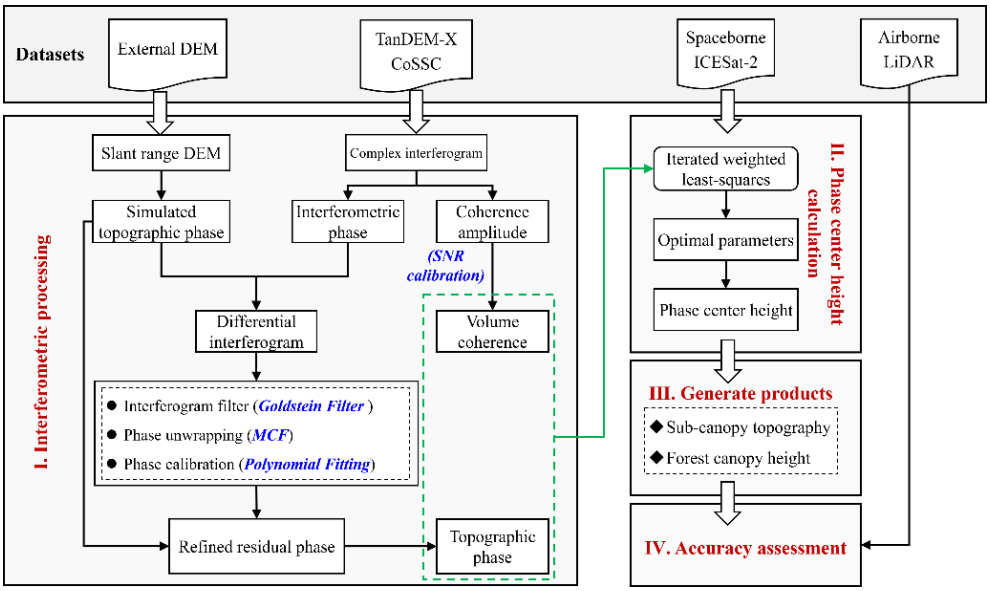

Fig. 2. Flowchart of the methodology proposed for estimation of sub-canopy topography and forest height.

to distinguish these areas from the taller forest areas. This threshold is set to the mean value of the overall coherence plus two times the standard deviation [30]. For pixels characterized by volume decorrelation greater than this threshold, we assume that a strong ground scattering contribution dominates the response, and the corresponding InSAR-based DEM elevation is directly used as the sub-canopy topography.

D. Accuracy Assessment

The accuracy of both topography and forest height products was evaluated utilizing Airborne Lidar Scanning (ALS) data. Two error measures were computed, namely the Bias (corresponding to the mean error) and root mean square error (RMSE). Furthermore, the coefficient of determination (R^2) was computed for each experiment. In the case of the topography verification, an additional standard deviation (STD) indicator was included. The calculation of these statistic indicators is detailed as follows:

$$Bias = n^{-1}\sum_{i=1}^{n}(X_i - Y_i) \tag{14}$$

$$RMSE = |n^{-1}\sum_{i=1}^{n}(X_i - Y_i)^2|^{\frac{1}{2}} \tag{15}$$

$$R^2 = 1 - \frac{\sum_{i=1}^{n}(X_i - Y_i)^2}{\sum_{i=1}^{n}(M - X_i)^2} \tag{16}$$

$$\mathrm{STD} = \left|(n-1)^{-1}\sum_{i=1}^{n}\left((X_i - Y_i) - Bias\right)^2\right|^{\frac{1}{2}} \tag{17}$$

where X is the measured value from radar, Y is the value from ALS measurement, and M is the mean of the ALS measurement values. Topography products are evaluated at the pixel scale, while forest height products are evaluated at the forest stand level (~1 hectare).

A detailed flowchart of the proposed method is shown in Fig. 2. Furthermore, the processing methods employed at several critical steps are highlighted in blue italics font. Specifically, to attain high-quality topographic phase, we conducted a multi-looking operation to suppress speckle noise during complex interferogram generation. Then, the interferogram was processed into a differential interferogram by removing the primary topographic component, for which we adopted TanDEM-X 90 m DEM as the external DEM. Subsequently, the resulting differential interferogram was subject to filtering using the Goldstein Filter [43] to reduce the influence of phase noise, and the filtered interferogram was unwrapped using the Minimum Cost Flow (MCF) algorithm [44]. Finally, we employed a polynomial fitting to refine the phase offsets caused by potential orbit inaccuracies [45]. Therefore, the resulting phase represents the refined residual phase with respect to the simulated topographic phase, and the total topographic phase can be obtained by combining these two components. The resulting total topographic phase was used as input for the sub-canopy topography inversion mode (see (11)). Additionally, a conventional InSAR-based DEM can be achieved by performing the phase-to-height conversion. Regarding the coherence amplitude, we compensated the SNR decorrelation to achieve the volume decorrelation using the sensor parameters and the method outlined in [16]. Regarding the resolution, all radar-based topography and forest canopy height products were geocoded and derived with a 12-m pixel spacing, consistent with that of the global TanDEM-X DEM product [17].

III. Test Sites and Datasets

A. Test Sites

To investigate the performance of our proposed approach, four forest sites (Fig. 3), characterized by different forest types (i.e., boreal, hemi-boreal, temperate, and tropical forests), terrain conditions (i.e., flat and rugged terrain), and climates, were selected. Krycklan catchment is located in northern Sweden, with elevations from 60 to 440 m above sea level

(*a.s.l.*) and moderate slopes. The characteristic vegetation of this boreal landscape is dominated by Norway spruce, Scots pine and fractions of birch, with a mean forest height of 18 m and a maximum height of 30 m at the stand scale. A second site located in Remningstorp in southern Sweden, includes small hills ranging from 120 m to 145 m. This is a hemi-boreal forest in which the prevailing species are also Norway spruce, Scots pine and birch, with a mean forest height around 20 m at the stand scale. A third test site is located in Yanguas (Spain), which is mainly covered with temperate coniferous tree species and a portion of deciduous broadleaved species (e,g., European beech), with a maximum tree height of about 35 m. Compared to the previous two sites, this region has a more fragmented topography with significant terrain slope variations, allowing us to investigate the impact of terrain slope on the proposed method. A fourth study area is located in Kango region

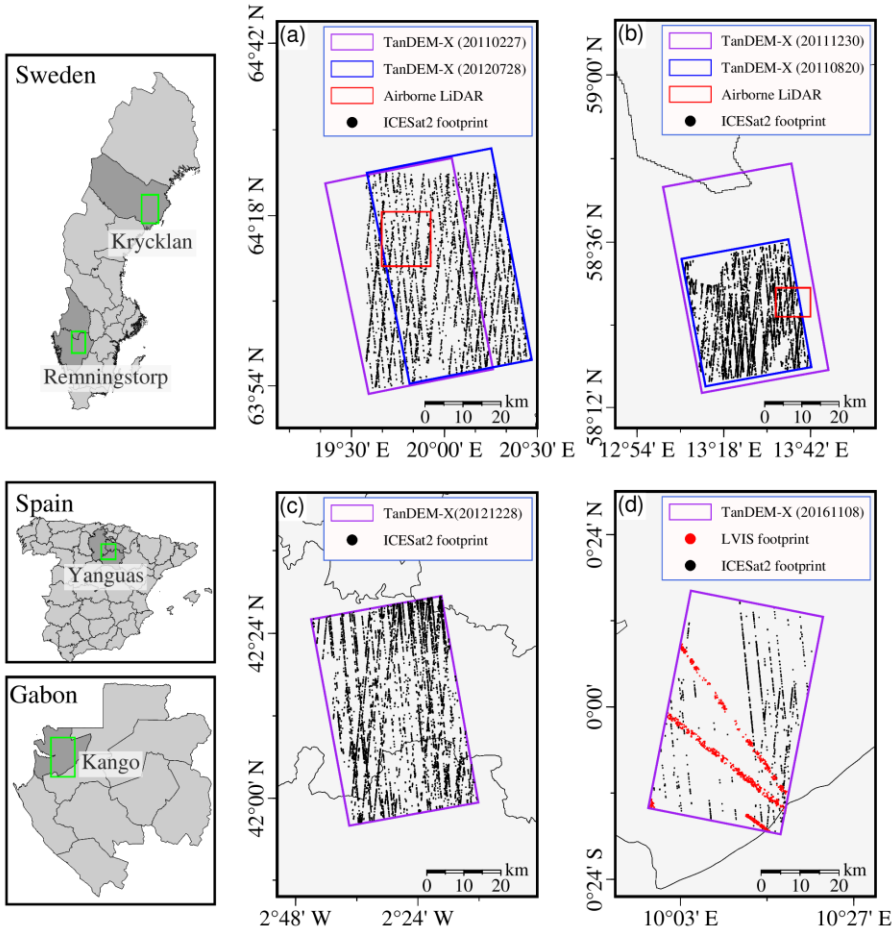

Fig. 3. Geolocation of the test sites: (a) Krycklan, (b) Remningstorp, (c) Yanguas, and (d) Kango. The footprints of the ICESat-2 points are represented by black dots.

TABLE I

SUMMARY OF TANDEM-X DATASETS EMPLOYED. θ IS THE NOMINAL INCIDENCE ANGLE, *HoA* DENOTES THE HEIGHT OF AMBIGUITY, Pol. STANDS FOR THE POLARIZATION MODE

Test site	Acquisition Date (yyyymmdd)	θ [°]	Effective baseline [m]	*HoA* [m]	Pol.
Krycklan	20110227	39	150.5	44.8	HH
	20120728	40	185.9	37.5	HH
Remningstorp	20111230	39	106.4	63.5	HH
	20110820	40	128.2	52.3	VV
Yanguas	20121228	31	151.1	36.3	HH
Kango	20161108	38	72.5	88.6	HH

(Gabon), which is covered with typical tropical forest with a mean forest height of approximately 40 m at the pixel scale.

Regarding the climatic conditions, the Krycklan catchment is in the subarctic climate zone, with an average temperature of 1.8℃ (1981-2010), while the mean temperatures in January and July are -9.5 and +14.7℃, respectively [46]. The cold winter temperatures lead to permanent frozen conditions during winter, therefore seasonal changes in the forest can be expected in this area [16]. Therefore, it is suitable to investigate the impact of different seasonal acquisitions on the proposed method. In contrast, Remningstorp site belongs to the temperate maritime climate with a mean temperature in winter around 0℃. Therefore, this site has a less winter conditions, which results in a less pronounced seasonality compared to the Krycklan test site [47]. The Mediterranean climate in Yanguas site gives rise to coniferous forests that lack pronounced seasonal characteristics, while the deciduous forests may exhibit some degree of seasonality. The Kango site is located in the tropical rainforest climate zone, with generally warm and humid conditions throughout the year, resulting also in minimal seasonal changes in the forest. For a more comprehensive understanding of the impacts of forest seasonality on TanDEM-X measurement in various forest ecosystems, refer to the literature [16].

B. TanDEM-X Acquisitions

We utilized single-polarization stripmap InSAR data gathered during winter and summer at the Krycklan and Remningstorp sites. Unfortunately, the summer acquisition in the Remningstorp test site was only available in VV polarization. Nevertheless, according to [16] and [47] the effect of the polarization (VV instead of HH) has minor effects in the interferometric phase, and therefore the results are comparable. For the Yanguas and the Kango sites, where the seasonal changes in the forests are less pronounced, we used only one data pair. The parameters of all the TanDEM-X data are listed in Table I.

C. Space-borne ICESat-2 Acquisitions

National Aeronautics and Space Administration (NASA) launched the ICESat-2 satellite in September 2018 with the aim of quantifying ice-sheet contributions to sea level change [48]. The mission carries a single instrument, the Advanced Topographic Laser Altimeter System (ATLAS), which produces multi-level and multi-category data products. In this study, we utilized the ATL08 product that provides elevation measurement for land and vegetation surfaces [49]. To ensure accurate ground reference data, we selected strong beam data acquired at night and removed any outliers with an estimated height uncertainty (the standard deviation of the ground elevation provided by the ATL08 product) greater than the average value. Furthermore, to accurately depict the relationship between PD and PCH, ICESat-2 measurement with forest canopy height (according to the derived canopy height "*h_canopy*") below 5 m were excluded. After these preprocessing steps, the final ICESat-2 dataset over each study area were obtained and marked by the black dots in Fig. 3, which were utilized to determine the unknown parameters in (6). Note that, since every ICESat-2 ATL08 point has a footprint of around 100 m by 11 m, a Gaussian weighting function is used to extract the average values of the raster data within the footprint of the point.

D. Airborne LiDAR Acquisitions

At the Krycklan site, the Swedish National Land Survey (Lantmäteriet) collected ALS data during the BioSAR2008 campaign [50]. The obtained data produced high-resolution DTM and forest height products, with resolutions of 1 m and 10 m, respectively. At Remningstorp, ALS measurement were performed on 29 August, 2010 [51], and DTM and forest height products were created with 0.5-m resolution. For the Yanguas site, ALS data were acquired between 2009 and 2015 as part of the Spanish National Territory Observation Program [52]. Based on these acquisitions, ALS-based DTM and CHM at 5-m resolution were created to cover the entire country. In addition, NASA obtained the high-precision LiDAR data over the Kango site during the AfriSAR campaign using the airborne full-waveform LVIS system [53]. To facilitate analysis and validation, all ALS data were resampled to the same resolution as the radar-based products (i.e., 12-m pixel spacing) using the nearest neighbor interpolation method.

Furthermore, it is noteworthy that there is a time gap between the acquisitions of TanDEM-X, ICESat-2 and ALS data. For the topography data, we can assume that the difference in space-borne ICESat-2 and airborne DTM measurements is negligible. Thus, these data can be utilized as reference data to support the solution of (11) and validate the derived products, and this time gap is not expected to be a major source of error that would limit the validity of the method described in this paper. When validating the radar-based forest height against ALS forest height data, it is important to consider the possibility that the forest conditions may have changed during this period due to tree growth.

IV. Experimental Results

A. Krycklan Test Site

1) Phase Center Height Calculation: To produce a wall-to-wall PCH map, volume coherence magnitude was utilized to estimate PDs. The PDs for both winter (Fig. 4(a1)) and summer (Fig. 4(b1)) acquisitions are mainly concentrated around 9 m. The enlarged maps of the ALS footprints indicate a maximum PD of 14 m in winter (Fig. 4(a2)) and around 11 m in summer (Fig. 4(b2)). Statistical results (Fig. 5) revealed a wider distribution of PD values in winter than in summer, and the PD values in summer concentrated mainly between 5 and 10 m. By applying (11) with sparse ICESat-2 ground elevation points, we established the linear relationship between the PDs and PCHs, which revealed a strong correlation between the two variables for both seasonal acquisitions, as clearly demonstrated in Fig. 6. Subsequently, the PCH at each pixel was calculated by exploiting the obtained fitting functions, which will be later used to produce the sub-canopy topography and forest canopy height products.

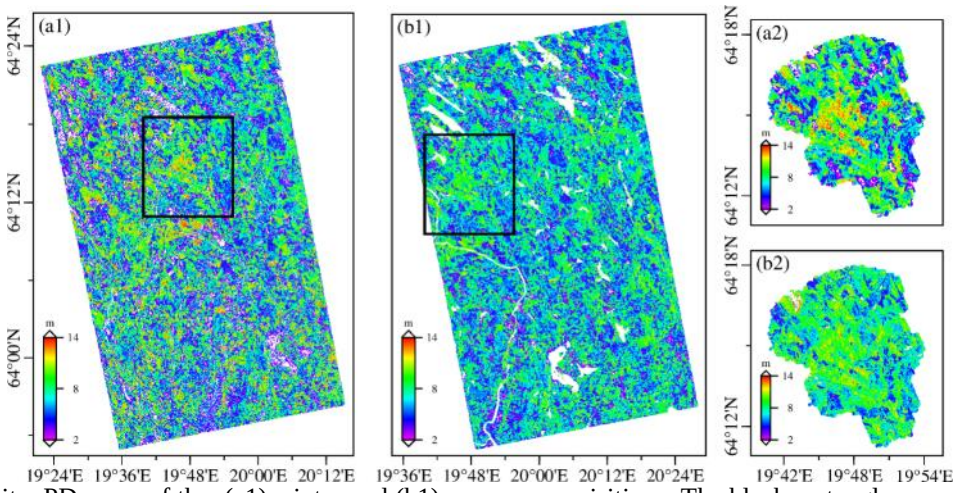

Fig. 4. Krycklan site: PD maps of the: (a1) winter and (b1) summer acquisitions. The black rectangles represent the coverage of the ALS data. (a2) and (b2) show the corresponding close-ups of the ALS footprint.

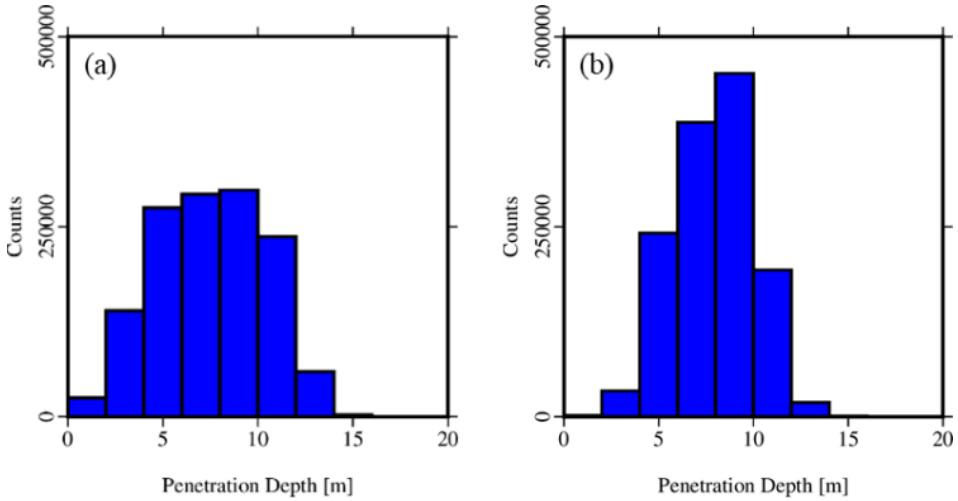

Fig. 5. Krycklan site: histogram of PDs over the ALS coverage area in: (a) winter and (b) summer acquisitions.

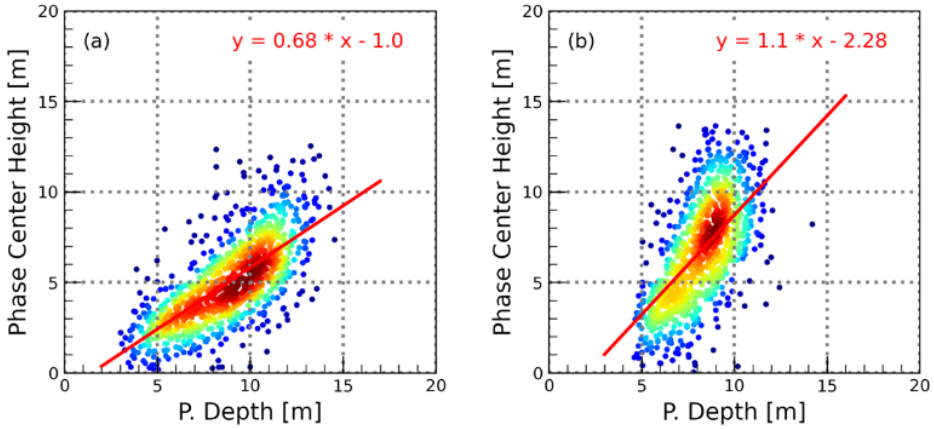

Fig. 6. Krycklan site: fitting plots between PD and PCH: (a) winter and (b) summer. The red lines denote the fitting solution.

2) Sub-canopy Topography Retrieval: By subtracting the estimated PCHs from the conventional InSAR-based DEM, we extracted the sub-canopy topography for the two seasonal acquisitions. It is worth noting that all terrain elevations in the resulting data are represented in meters relative to the WGS84-ellipsoid surface.

Figures 7(a) and (b) show the InSAR-based DEM of the

winter acquisition and the derived sub-canopy topography, respectively. The associated elevation error maps with respect to the ALS DTM (as indicated by the black rectangle) are shown in Figs. 7(c) and (d). The conventional TanDEM-X InSAR DEM is significantly higher than the ALS DTM due to the presence of forest height signals. Conversely, our approach effectively corrects the forest's influence, resulting in a sub-canopy topography that exhibits improved alignment the ALS DTM, as demonstrated by the reduced residual elevation errors (Fig. 7(d)). Moreover, these residual elevation errors do not display a noticeable trend or spatial dependence.

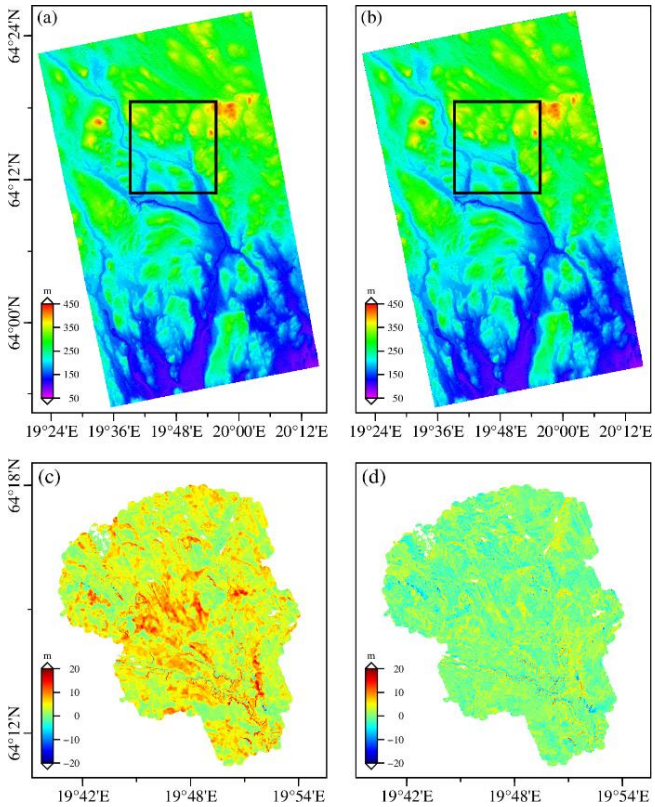

Fig. 7. Krycklan site (winter scenario): (a) InSAR-based DEM, (b) Sub-canopy topography, and the associated elevation error maps with respect to the ALS DTM in (c) and (d). The black rectangles in (a) and (b) indicate the coverage of the ALS measurement.

The scatterplots of topography for the winter acquisition are shown in Fig. 8, which provide a quantitative comparison between the radar-based DEMs and ALS DTM. We observe that, the InSAR-based DEM exhibits a positive bias (higher than 4 m). In contrast, the sub-canopy topography derived via our approach is much closer to the ALS DTM showing a 2.45 m RMSE (i.e., reduced by more than 50%) and a very small average bias (-0.41 m). Moreover, the sub-canopy topography displayed a decreased STD value of 2.42 m compared to the conventional InSAR DEM, which had a STD of 2.70 m.

Figures 9 (a) and (b) depict both the InSAR-based DEM and the sub-canopy topography for the summer acquisition, with the associated elevation error maps compared to the ALS DTM shown in Figs. 9(c) and (d). Similar to the results obtained during the winter acquisition, the conventional TanDEM-X InSAR DEM exhibits noticeable elevation errors caused by the forest height, and these errors are more pronounced compared in the winter acquisition (see Fig. 7(c)), due to the increased forest volume scattering during the summer season. Regarding the sub-canopy topography for the summer acquisition, as depicted in Fig. 9(b), it demonstrates a notably lower elevation errors with respect to the ALS DTM (see Fig. 9(d)). Nevertheless, it is apparent that the residual elevation errors are more pronounced than those observed in the winter acquisition.

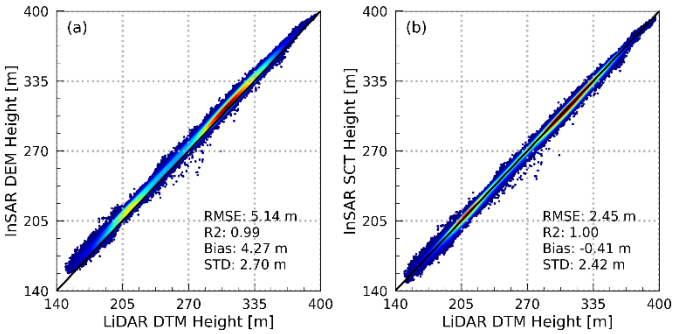

Fig. 8. Krycklan site elevation validation (winter scenario): ALS DTM versus (a) InSAR-based DEM and (b) sub-canopy topography (SCT).

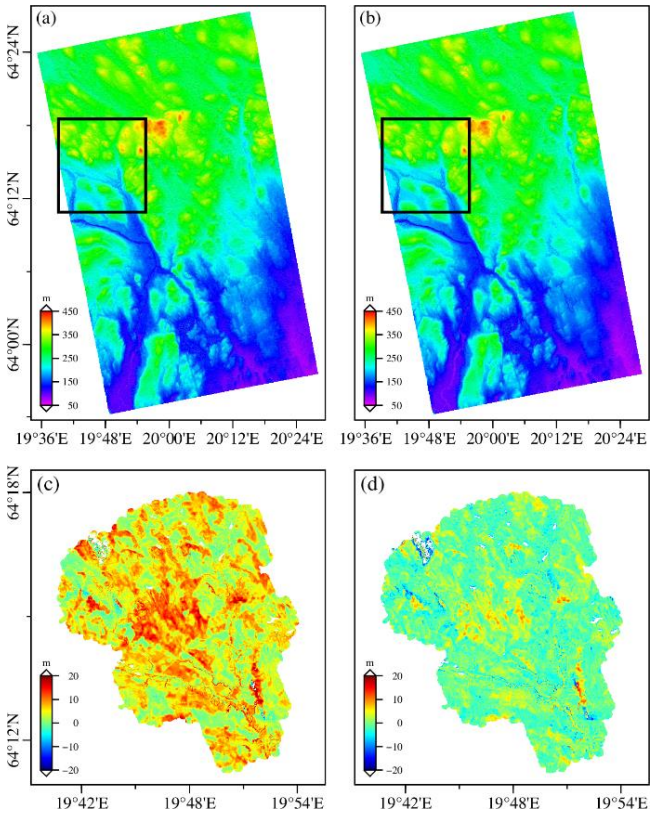

Fig. 9. Krycklan site (summer scenario): (a) InSAR-based DEM. (b) sub-canopy topography, and the associated elevation error maps with respect to the ALS DTM in (c) and (d). The black rectangles in (a) and (b) indicate the coverage of the ALS measurement.

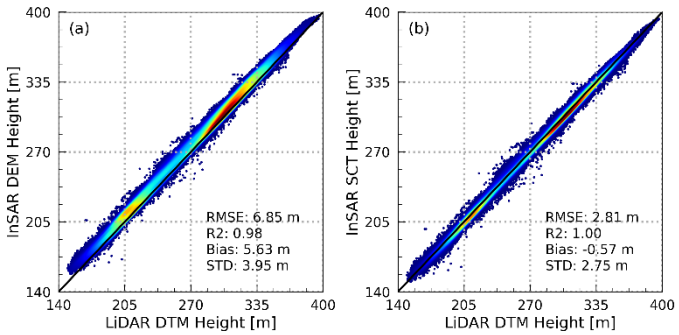

Fig. 10. Krycklan site elevation validation (summer scenario): ALS DTM versus (a) InSAR-based DEM and (b) sub-canopy topography (SCT).

To further evaluate these topography products, a quantitative comparison between the obtained DEMs and the ALS DTM is presented in Fig. 10. In this case the InSAR-based DEM shows a 6.85 m RMSE and a 5.63 m bias relative to the ALS DTM, whereas the sub-canopy topography derived by the proposed method significantly improves the accuracy: an RMSE of 2.81 m and a bias of -0.57 m. Furthermore, there is a reduction in the STD value by 1.2 m compared to the conventional InSAR DEM.

3) Forest Height Retrieval: Finally, forest canopy height is retrieved by combining the estimated PD and PCH components. In Fig. 11, the forest height results and validation plots for the winter scenario are presented. The forest canopy height estimation shows a reasonable agreement with the ALS forest height, with an RMSE value of 2.7 m. This method is particularly effective for short and young forest stands with heights less than 15 m, but it tends to overestimate the height for taller stands. The overall bias of the resulting forest height is 0.48 m with respect to the ALS product.

The results for the summer scenario are presented in Fig. 12. The derived forest height is generally overestimated, since there is an offset of around 0.8 m between the radar and ALS measurements, but the RMSE is below 3 m. Therefore, the proposed method is effective in generating forest height product

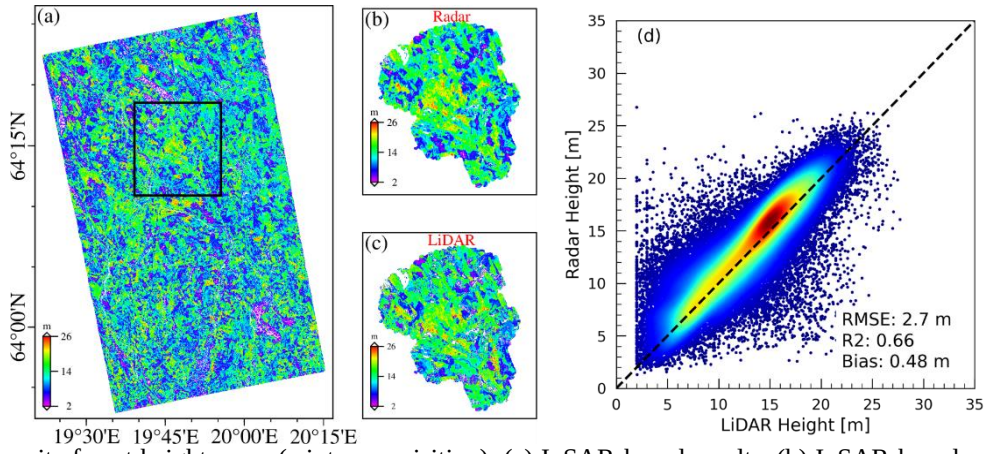

Fig. 11. Krycklan site forest height maps (winter acquisition): (a) InSAR-based results. (b) InSAR-based result matching the coverage of ALS data, marked by the black rectangle in (a). (c) ALS forest height. (d) Density scatterplot of radar and ALS height.

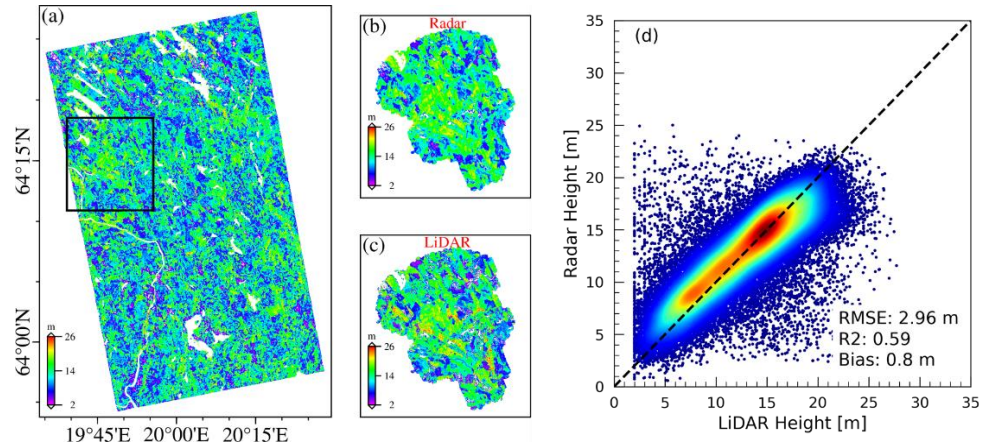

Fig. 12. Krycklan site forest height maps (summer acquisition): (a) InSAR-based results. (b) InSAR-based results matching the LiDAR coverage, marked by the black rectangle in (a). (c) ALS forest height. (d) Density scatterplot of radar and ALS height.

using single-baseline InSAR data, even without an available DTM.

B. Remningstorp Test Site

1) Sub-canopy Topography Retrieval: Figure 13 shows the histograms of the PD results in both seasons, which are very similar but with values slightly lower in summer than in winter. Compared to the Krycklan site, the Remningstorp test site experiences less pronounced winter conditions, so the slight changes in the PD are mainly induced by falling leaves or slightly different weather conditions. Next, in the estimated linear function between PD and PCH (Fig. 14), we observe a slightly stronger saturation in summer than in winter, so a lower inversion accuracy can be expected during summer scenario.

Regarding the comparison of the derived sub-canopy topography and the reference ALS DTM, in the scatterplots for the winter scenario (Fig. 15) the sub-canopy topography yields an RMSE of 3.83 m, which is 50% better than the InSAR-based DEM (RMSE=7.95 m). Similarly, for the summer scenario (Fig. 16), the obtained RMSE is 4.52 m, instead of 8.54 m for the InSAR-based DEM. Furthermore, the resulting bias in winter is only 0.05 m, whereas in summer it is 0.62 m. When concerning the STD, the sub-canopy topography reflects an approximate reduction of 1 m across both seasonal cases.

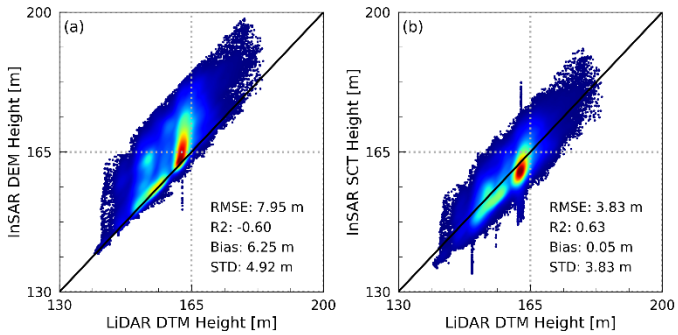

Fig. 15. Remningstorp site elevation validation (winter scenario): ALS DTM versus (a) InSAR-based DEM and (b) sub-canopy topography (SCT).

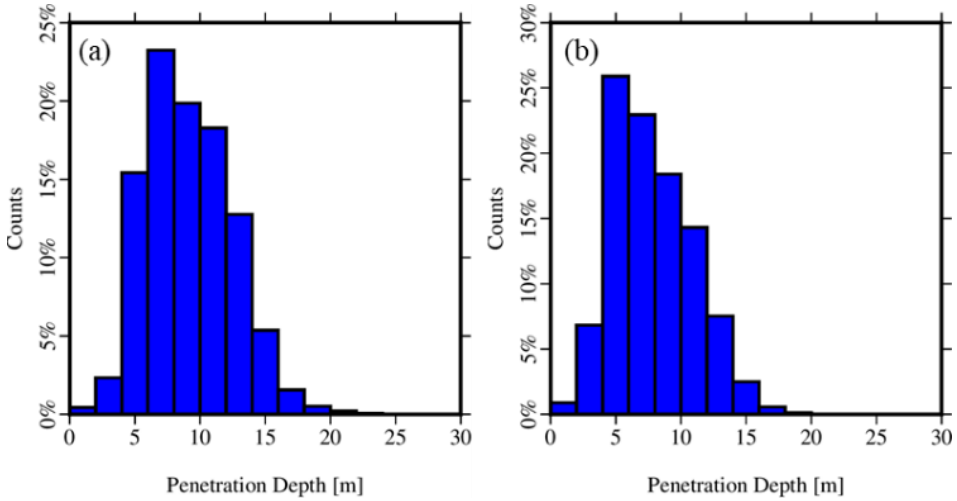

Fig. 13. Remningstorp site: histogram of PDs in: (a) winter and (b) summer acquisitions.

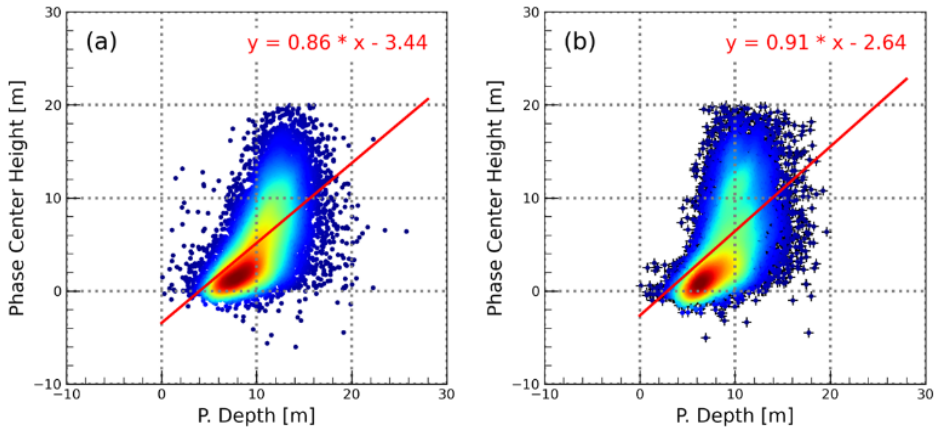

Fig. 14. Remningstorp site: fitting plots between PD and PCH: (a) winter and (b) summer. The red lines denote the fitting solution.

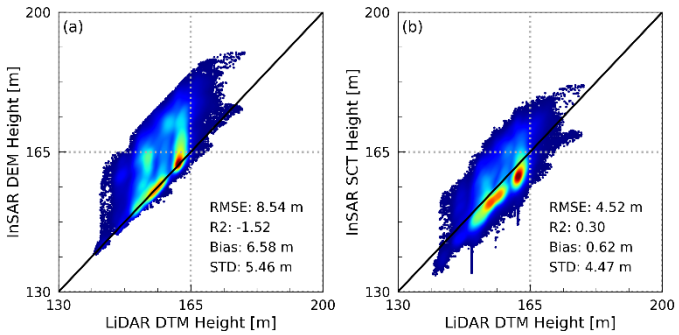

Fig. 16. Remningstorp site elevation validation (summer scenario): ALS DTM versus (a) InSAR-based DEM and (b) sub-canopy topography (SCT).

2) Forest Height Retrieval: Figure 17 shows the total forest height for the winter scenario at the Remningstorp test site, as well as its comparison with the ALS forest height product. The scatterplot (Fig. 17(d)) indicates that the radar-derived forest height reasonably agrees with the ALS values, with an RMSE of 3.33 m and an average bias of 0.76 m. However, we also notice that short forest stands tend to be overestimated, while taller forest stands appear to be well estimated. This acquisition is characterized by a smaller baseline, compared to the previous results (see Table 1), which justifies a better sensitivity to taller than to shorter trees in this case [24].

Figure 18 displays the total forest height for the summer acquisition, where some clear differences are found with respect to the winter case. For instance, forest height is underestimated, especially for tall forest stands, even though it correlates with spatial variations of height very well. This phenomenon could be explained by an insufficient penetration caused by increased density or changed dielectric properties of the canopy layer in summer, which causes the interferometer not to see the entire forest volume. The quantitative comparison between the ALS and radar-based height (Fig. 18(d)) shows that the radar-based forest height has an average bias of -0.69 m and an RMSE of 3.84 m, hence with lower accuracy than that of the winter scenario (Fig. 17).

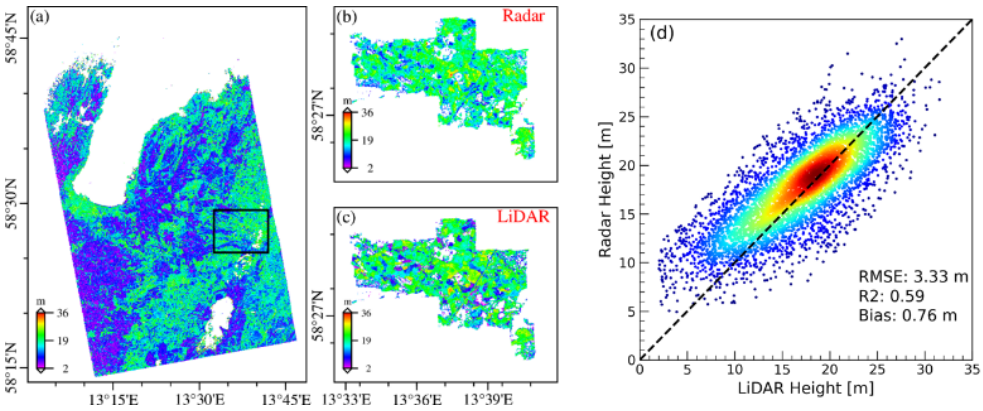

Fig. 17. Remningstorp site forest height (winter scenario): (a) InSAR-based canopy height. (b) InSAR-based result matching the coverage of ALS measurement, marked by the black rectangle in (a). (c) ALS forest height. (d) Density scatterplot of ALS and radar measurements.

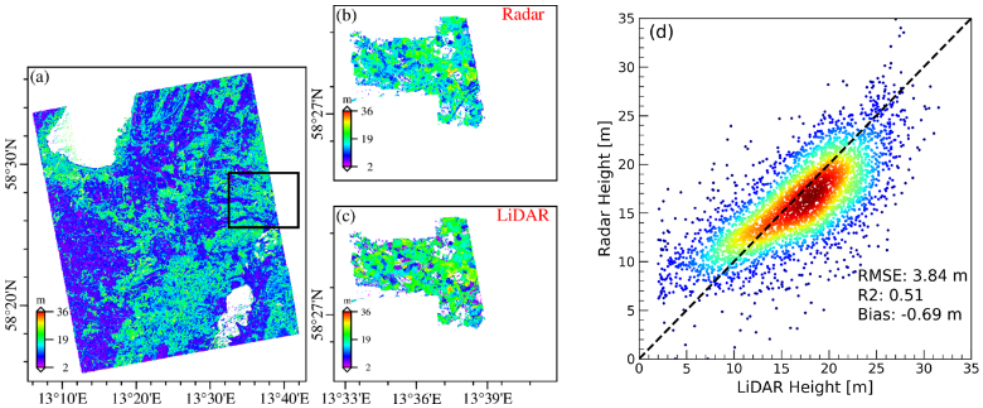

Fig. 18. Remningstorp site forest height (summer scenario): (a) InSAR-based canopy height. (b) InSAR-based result matching the coverage of ALS measurement, marked by the black rectangle in (a). (c) ALS forest height. (d) Density scatterplot of ALS and radar measurements.

C. Yanguas Test Site

The scatter plot between PD and PCH is presented in Fig. 19, which indicates a clear relationship between these two variables, thereby the estimated PD can be used as a good proxy for the PCH calculation in this area. To compare the conventional InSAR-based DEM and the derived sub-canopy topography, the associated elevation error maps with respect to the ALS DTM, that covers the entire SAR scene, are shown in Fig. 20. The proposed method effectively removes forest height signals and produces a sub-canopy topography with a small residual elevation error (see Fig. 20(d)). The quantitative evaluation results, presented in Fig. 21, show that the proposed method eliminates almost completely the bias and enhances the accuracy of topography estimation, resulting in a decrease in RMSE by ~1 m and a decrease in STD by 0.7 m. Compared to the Krycklan and Remningstorp test sites, the smaller increase in RMSE at this test site is mainly due to the lower proportion of forest areas. However, by focusing on the areas with forest height greater than 5 m, the RMSE is reduced from 6.67 m to 4.27 m, representing an improvement of 35%.

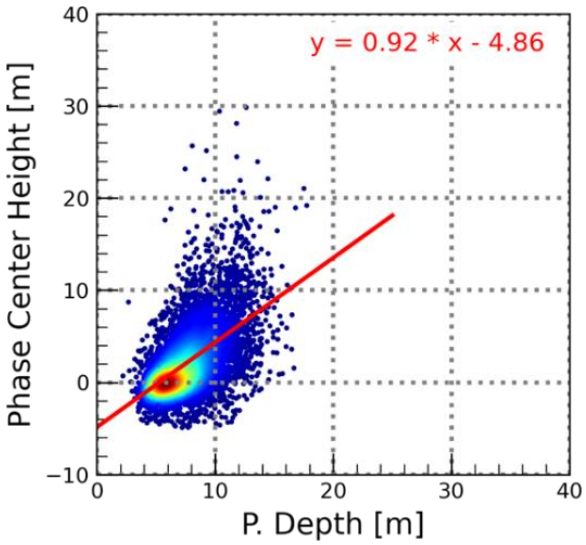

Fig. 19. Yanguas site: fitting plots between PD and PCH.

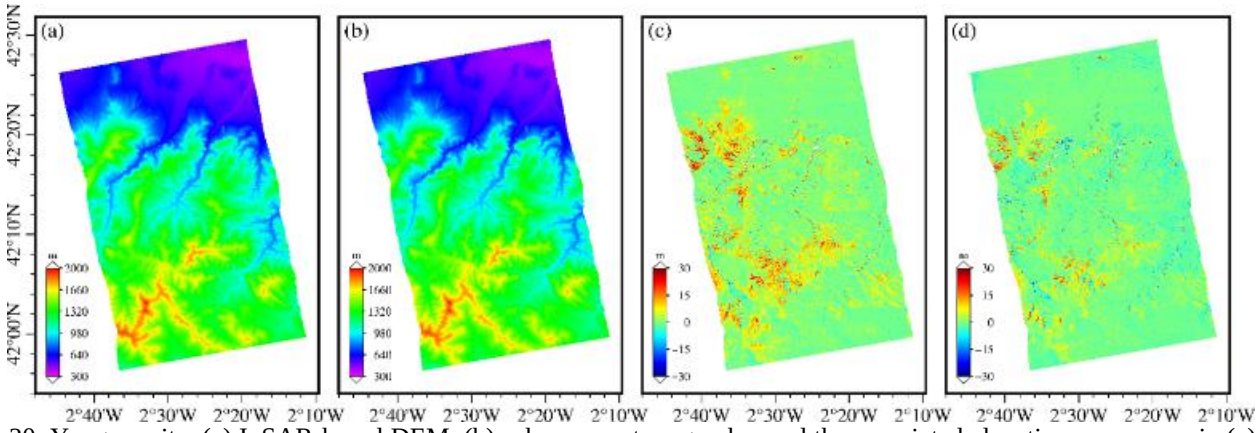

Fig. 20. Yanguas site: (a) InSAR-based DEM, (b) sub-canopy topography, and the associated elevation error maps in (c) and (d).

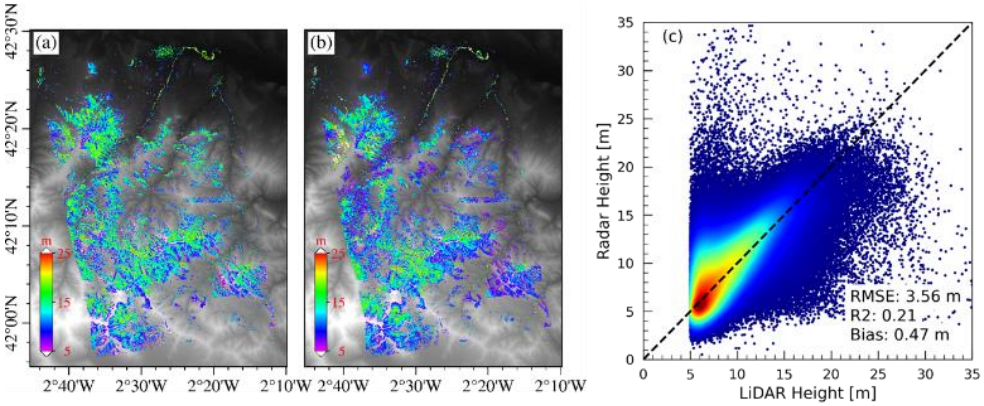

Fig. 22. Yanguas site forest height maps: (a) radar-based forest height. (b) ALS forest height. (c) Density scatterplot of ALS and radar measurements.

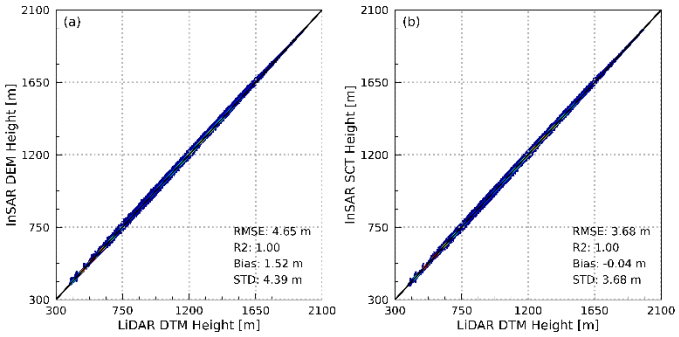

Fig. 21. Yanguas site elevation validation: ALS DTM versus (a) InSAR-based DEM and (b) sub-canopy topography (SCT).

In Fig. 22, radar-based and ALS forest height at the Yanguas test site are presented. The radar-derived forest height generally corresponds well to the ALS measurements, with an RMSE of 3.56 m. However, the scatterplot in Fig. 22(c) reveals that some short forest stands were overestimated by this method. This result can be explained by two possible reasons. Firstly, the radar signal may penetrate deeper into the forest understory in areas with sparse vegetation, leading to an overestimation of the forest height. Secondly, the radar signal may be affected by the presence of terrain slopes.

D. Kango Test Site

Based on the fitting plots between PD and PCH (Fig. 23) and the InSAR-based DEM (Fig. 24(a)), the sub-canopy topography was derived and shown in Fig. 24(b). For a detailed comparison, a small area marked by the red rectangle in Fig. 24 is shown in Fig. 25. In Fig. 25(a), the optical image reveals an obvious boundary dividing a tall forest stand and a short vegetation area, in which the InSAR-based DEM shows a noticeable elevation offset, whereas this jump disappeared in the sub-canopy topography. Additionally, the sub-canopy topography exhibits more detailed terrain features than the conventional InSAR-derived DEM.

Quantitatively, in comparison to the LVIS ground data, the InSAR DEM is characterized by an RMSE of 22.5 m, while the sub-canopy topography provides a more accurate estimation of topography with an RMSE of 9.52 m (refer to Fig.26), and the PCH removes partially the elevation bias induced by forest height, albeit with a smaller reduction in STD. To explore the reason behind this finding, we analyzed the scatterplots between the forest height and interferometric coherence magnitude, and between forest height and PCH. Figure 27(a) shows that coherence lacks the necessary sensitivity to variations in forest height due to insufficient penetration of X-band microwave signals. An interesting observation is the presence of a distinct linear correlation between forest height

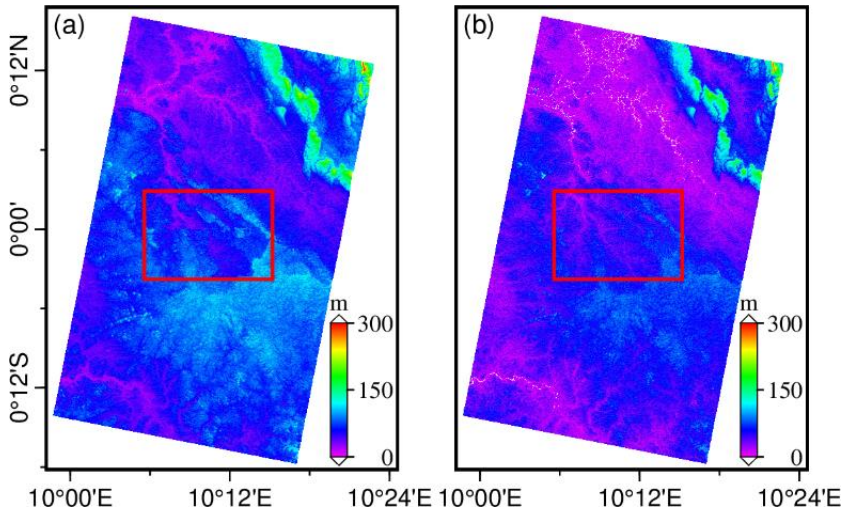

Fig. 24. Kango site: (a) InSAR-based DEM, (b) sub-canopy topography.

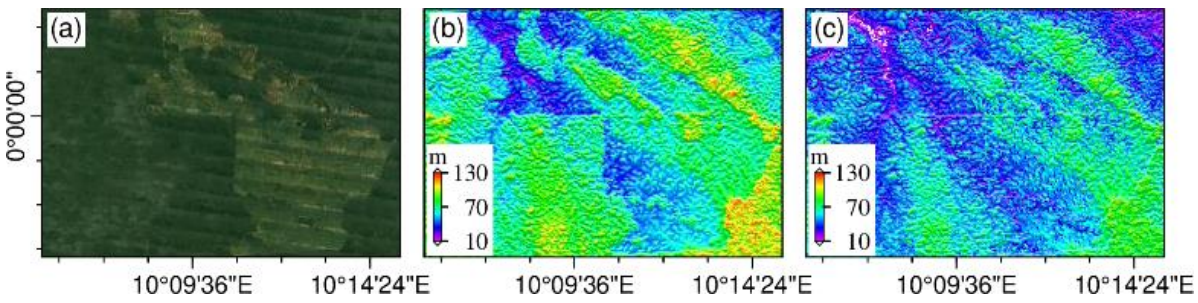

Fig. 25. DEM close-ups of the sample area in Figs. 24: (a) optical image, (b) InSAR-derived DEM, (c) sub-canopy topography.

and PCH (see Fig. 27(b)), a phenomenon that was also demonstrated in [21], [22], [23]. This finding holds potential for the development of new algorithms to address topographic mapping challenges in denser tropical forest scenarios.

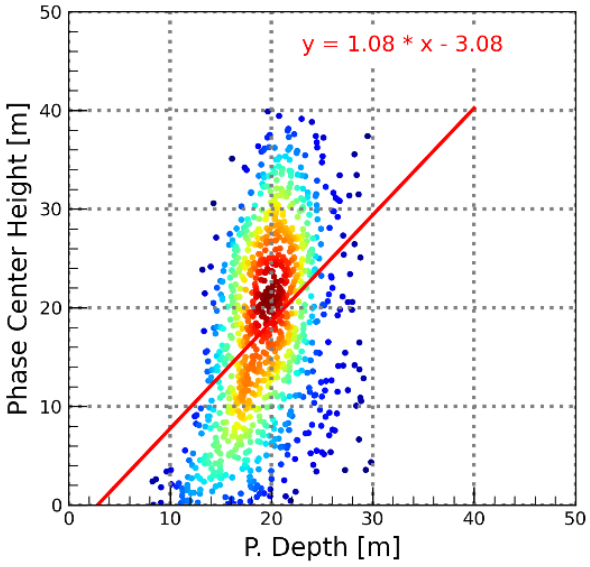

Fig. 23. Kango site: fitting plots between PD and PCH.

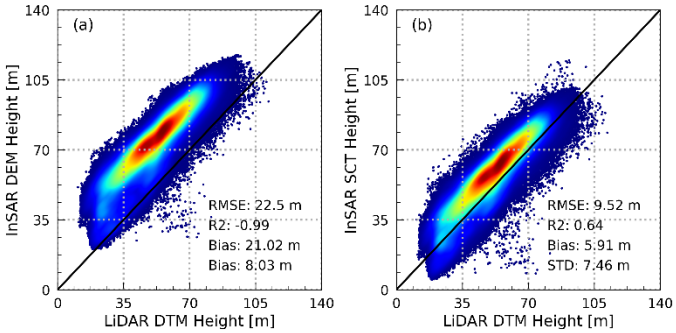

Fig. 26. Kango site elevation validation: LVIS ground elevation versus (a) InSAR-based DEM and (b) sub-canopy topography (SCT).

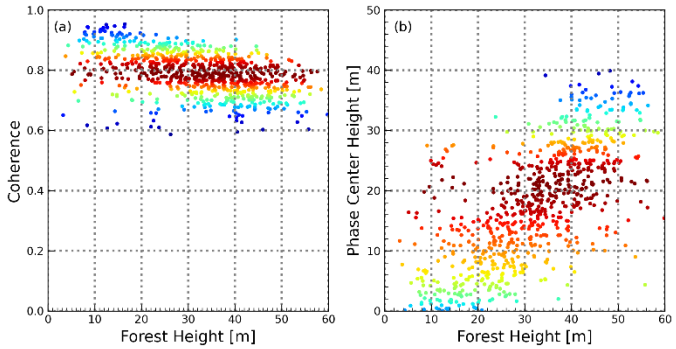

Fig. 27. Kango site scatterplots for: (a) Forest height versus coherence magnitude, and (b) Forest height versus phase center height (PCH).

V. Discussion

In this work, we propose a novel InSAR processing framework that enables the simultaneous estimation of sub-canopy topography and forest canopy height. Our approach leverages single-baseline single-polarization TanDEM-X InSAR data complemented by sparse ICESat-2 ground data. In contrast to previous research [30], [31], we introduce a technique that exploits a linear function correlation between PD (Penetration Depth) and PCH (Phase Center Height), by incorporating the SINC-model based on the coherence amplitude. This modification in the InSAR phase model results in an enhanced method for estimating sub-canopy topography, although its performance depends on the forest conditions. Furthermore, our approach enables the simultaneous estimation of forest height. Another novelty of our work is the inclusion of ICESat-2 ground data, which serve as reliable ground control points. These data assist in the model solution and help calibrate the possible systematic errors associated with imprecise orbital parameters [54]. To comprehensively evaluate the proposed method, we assessed the impact of various data acquisition conditions, including forest types/structure, terrain, and climate or forest seasonality, by conducting experiments at four distinct test sites. These investigations confirm that it is feasible to produce the sub-canopy topography and to provide wall-to-wall estimation of forest height using the proposed method with single-baseline single-polarization TanDEM-X InSAR data. Furthermore, the copious earth observation data available from TanDEM-X and space-borne LiDAR (e.g., NASA's ICESat-1/-2 and GEDI) allow us to broaden the applicability of the proposed approach to large-scale scenarios. However, it should be noted that the method may encounter challenges in dense forest stands (e.g., dense tropical forest scenario).

A. Comparison between the Proposed Method and Existing Methods

By testing the proposed method in various forest ecosystems, its effectiveness has been demonstrated, except for the stands with very dense canopy. To further assess its suitability and advantages for simultaneous sub-canopy topography and forest height inversion, we conducted here a comparative analysis between our approach and existing methods, for which we chose the Krycklan test site as a representative example. The Krycklan forest area is a well-established forest location commonly used for testing methods related to topography and forest parameters inversion, using airborne [10], [55] and space-borne SAR data [11], [16], [31], [47], [56].

In terms of the sub-canopy topography retrieval, our approach demonstrated an improved performance at the Krycklan test site, achieving an RMSE of 2.45 m, which is better than the RMSE of 3.22 m previously reported for the same test site in [31]. This may have two possible explanations. In the approach described in [28], a two-step PCH estimation strategy was employed. This process involved initially estimating the forest height by fitting a linear function between ICESat-2 forest height and the PD, and subsequently, calculating the PCH by subtracting the PD

from the resulting forest height. In our approach, we establish a direct relationship between the PCH and PD using a linear function, and the function was integrated into the InSAR phase model for the sub-canopy topography retrieval. This integration overcomes the limitation of a simplified scattering model based on coherence amplitude, which does not take into account on the interferometric phase [57]. As a result, it leads to a more accurate estimation of the PCH. On the other hand, in our approach, the utilization of ICESat-2 ground points provides a highly accurate elevation reference for calibrating the residuals in InSAR DEM. Comparing our approach to that of [11], which reported sub-canopy topography obtained by combining dual-baseline TanDEM-X data with the two-level model (TLM) and achieved an overall bias of less than 1 m with respect to the ALS DTM, our results are comparable to theirs, but obtained with single-baseline TanDEM-X data.

Furthermore, upon comparing the spatial distribution of the residual topography errors of the conventional InSAR-based DEMs (Fig. 7(c) and Fig. 9(c)) with the ALS forest height (Fig. 11(c)), it is clear that the spatial distribution of topography errors depends on forest height, which hence needs to be considered for improving the sub-canopy topography estimation. To validate this observation, we conducted a two-part analysis in which we compared our approach with the removal of a constant offset, in the following manner: (1) the average bias between the conventional InSAR-based DEM and ALS DTM at all DTM pixels was computed, and, considering it as a constant offset, it was removed from the conventional InSAR-based DEM; and (2) in the same way, but only for pixels with a forest height greater than 8 m (in the reference ALS forest height data). The summarized statistics of the results are presented in Table II. It is evident that while correcting a constant bias can reduce the RMSE to a certain extent, the improvement remains limited because such a processing strategy does not take into account the spatial variation in forest height. Additionally, in practical applications, it would be challenging to determine that offset value in absence of a high-resolution DTM and forest height product. In contrast, our approach leverages coherence magnitude to incorporate information on changes in both forest height and spatial distribution, resulting in a notable improvement in accuracy (i.e., RMSE and STD). Consequently, the simultaneous reduction in RMSE, bias, and STD confirms that our approach is more effective than a simple constant bias correction.

In comparison to the conventional forest height estimation method relying on the SINC-model [24], [58], our approach demonstrates superior performance, as illustrated in Fig. 11(d) and Fig. 12(d). The conventional inversion method consistently

TABLE II
SUMMARY OF THE ACCURACY FOR VARIOUS TOPOGRAPHY PRODUCTS IN THE KRYCKLAN TEST SITE

Acquisition season	Topography product	All pixels			Forest height >= 8 m		
		Bias [m]	RMSE [m]	STD [m]	Bias [m]	RMSE [m]	STD [m]
Winter	InSAR DEM	4.27	5.14	2.70	4.56	5.26	2.63
	Correction of constant offset	0	2.70	2.70	0	2.63	2.63
	Our method	-0.41	2.45	2.42	-0.07	2.18	2.18
Summer	InSAR DEM	5.63	6.85	3.95	6.14	7.23	3.83
	Correction of constant offset	0	3.95	3.95	0	3.83	3.83
	Our method	-0.57	2.81	2.75	-0.25	2.90	2.89

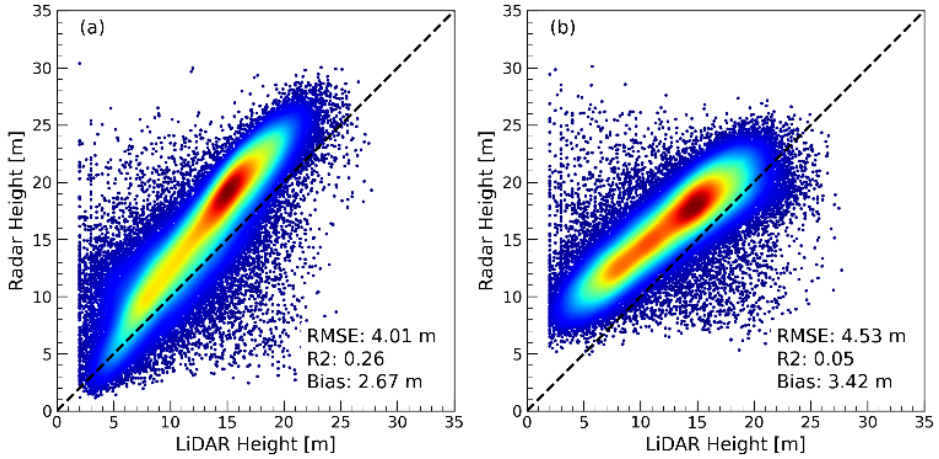

Fig. 28. Validation of forest height: radar-based forest height derived via the SINC-model in [23] vs ALS forest height: (a) winter scenario, and (b) summer scenario.

overestimates forest height across nearly all forest stands, as shown in Fig. 28. This can be attributed to the strong assumption of the conventional method (i.e., the phase center height typically lies around half of the canopy top height), while [16] reported that the penetration depth in the majority of forest stands at this test site were higher than half of the canopy height. Therefore, some studies suggest that using an empirical correction function may potential improve estimation [11], [25], [28], [57]. When it comes to our approach, although we also utilized the SINC-model to characterize the scattering of microwaves within the forested area (i.e., the estimation of the PD), an empirical linear model is employed to estimate the PCH, considering the variations in forest scenarios.

When compared to the method that combines TanDEM-X with LiDAR waveforms [28], [29], our approach offers the advantage of applicability to any geographical sites. This is because the current GEDI instrumentation is designed to collect data between 51.6° S and 51.6° N latitudes. However, a drawback of our approach is that, to force a balanced inversion of (6), we employed a constant vertical reflectivity function represented by $f(z) = 1$. This could be insufficient to depict the scattering distribution patterns of all forest scenarios. Therefore, further research is necessary to verify this issue.

B. Effects of Forest Conditions and Seasonality

The effectiveness of the proposed method relies on the ability of X-band to penetrate forest vegetation. In boreal (Krycklan) and hemi-boreal (Remningstorp) forest sites, we observed a strong correlation between PD and PCH, enabling accurate wall-to-wall estimation of PCH from PD. Moreover, a distinct seasonal dependence was noticed with summer and winter acquisitions at the two test sites. Notably, the winter acquisitions outperformed the summer acquisitions in the inversion accuracy. Previous studies [16] and [47] attributed these seasonal differences to the lower attenuation during winter season, which allows the radar to 'see' the entire forest volume. Furthermore, when considering the difference in the forest structures between these two test sites, our results indicated that the Krycklan test site, characterized by a homogeneous forest, consistently achieved higher inversion accuracy for both topography and forest height. In the case of dense tropical scenarios (e.g., Kango test site), which are usually characterized by taller trees with denser canopy than boreal forest, the limited penetration at X-band leads to a reduced sensitivity to variations in forest height, causing coherence to saturate. [16] reported similar results to our findings in the dense tropical forests of the Mawas test site (Indonesia). In this case, describing forest height variation solely based on coherence amplitude becomes unfeasible. This allows concluding that X-band InSAR data may not be suitable for extracting sub-canopy topography and/or forest height using the proposed method at forest scenarios with very dense canopy.

It is important to note that, this issue also arises in the denser forest stands within other forest ecosystems (e.g., boreal forest). For instance, a coherence saturation phenomenon can be observed in the summer acquisition at the Krycklan test site (Fig. 6(b)), resulting in significant residual elevation errors, as depicted in Fig. 9(d). In addition to the limitation imposed by the TanDEM-X measurement, a more significant impact may result from a single-baseline observation, since a single *HoA* cannot provide sufficient sensitivity to all forest height values present in the scene, as discussed in next subsection and highlighted in [24].

C. Limitations and Improvements for Future Work

First, when comparing the results from our four test sites, the Krycklan site exhibited the highest overall inversion accuracy. Lower accuracy at Remningstorp and Yanguas can be attributed to a mismatch between the model and the forest scene. Variations in forest structure, both horizontally and vertically, can impact the relationship between PD and PCH, thereby challenging the initial hypothesis of a linear relationship between these two variables. Additionally, it is noteworthy that X-band penetration does not increase indefinitely with increasing forest height, as indicated in Fig. 6 and Fig. 15. Beyond a certain critical point, the sensitivity to forest height variation decreases due to the insufficient penetration at X-band, as previously mentioned. In such cases, although a non-linear model could theoretically enhance the description of the relationship between PD and PCH, its performance is sensitive to the quality of ICESat-2 ground data and relies on strong manual intervention. On the contrary, combining the linear model with the iterated weighted least-square (IWLS) method maintains a stable solution for (11) and performs better. Nevertheless, our results revealed that a single fitting function is inadequate for accurately describing the relationship between PD and PCH for every pixel of a whole image. Therefore, to better account for the heterogeneity present in larger areas, we recommend modeling based on forest types and smaller regions, assuming less variation in forest conditions in these cases.

Second, in this study, we utilized only one pair of SAR images for each test case to evaluate our approach. Therefore, beyond the constraints related to the scattering model, there could be a potential limitation associated with the InSAR observation geometry, particularly the vertical wavenumber (or height of ambiguity), which directly determines the sensitivity of the observed data to forest parameters [59]. Regarding this issue, [60] investigated the influence of an optimized range of vertical wavenumber on the performance of forest height estimation and demonstrated that the interferometric coherence of a single baseline has an associated interval of successful inversion which depends on the vertical wavenumber. When focusing on our approach, an appropriately chosen baseline could provide a better distinction among different forest height classes, thereby improving the modeling and the inversion accuracy. In a future work, if multiple acquisitions are available, there is potential to enhance the results by a preselection of the most suited baseline for each study area.

Finally, the performance of the inversion process is also influenced by the quality of the phase, which directly impacts the accuracy of the conventional InSAR-based DEM.

Furthermore, in the case of single-baseline TanDEM-X acquisition, terrain slope becomes one of primary sources of error as it modifies the scattering components of the forest that contribute to the overall response of the microwave signals. It should be noted that different slope directions in range produce varying effects. To address this issue, a commonly employed technique is to combine multi-pass observations (e.g., ascending and descending) to compensate for the limitations of single-pass InSAR [61].

Based on these limitations, future research will focus on a modeling that incorporates forest diversity, multiple baseline data, and also multi-pass data to overcome sub-canopy topographic mapping challenges in mountainous regions. As a final comment, the unique characteristics of very dense forest scenarios will require the development of alternative approaches to improve accuracy and reliability. Moreover, in this study, to benchmark the resolution specifications of the global TanDEM-X DEM (i.e., 12 m), approximately 36 looks were used for interferogram derivation and coherence estimation. Nonetheless, using fewer looks (e.g., 2- to 4-look) may be beneficial for enhancing the sensitivity of X-band microwave to denser forest conditions by capturing forest gaps more effectively [12], [30], which requires further research.

V. Conclusion

In this work, we introduce a novel InSAR processing workflow that enables the simultaneous estimation of both sub-canopy topography and canopy height, utilizing single-baseline single-polarization TanDEM-X InSAR data, augmented by sparse measurements from the ICESat-2 mission. To validate the effectiveness of our method, we conducted experiments using TanDEM-X data collected over four distinct test sites, each characterized by varying forest types, terrain conditions, and climates. The experimental results demonstrate that, except for dense tropical forests or stands, our proposed method successfully extracts sub-canopy topography and forest height using single-baseline single-polarization TanDEM-X data. Furthermore, a single fitting function is inadequate for accurately describing the relationship between Penetration Depth (PD) and Phase Center Height (PCH) for every pixel of a whole image. Comparing the results of different seasons indicates that, for boreal and hemi-boreal forests, winter acquisitions proved to be more suitable for inversion compared to summer acquisitions.

Acknowledgment

The TanDEM-X CoSSC data were kindly provided by DLR (Projects NTI-INSA7497, OTHER7349). ICESat-2 ATL08 data were acquired from the NSIDC. LVIS datasets were provided by the Land, Vegetation and Ice Sensor (LVIS) team in Code 61A at NASA Goddard Space Flight Center with support from the University of Maryland, College Park. The TanDEM-X 90m DEM data were provided by DLR.

References

[1] A. M. AL-Areeq *et al.*, "Digital elevation model for flood hazards analysis in complex terrain: Case study from Jeddah, Saudi Arabia," *Int. J. Appl. Earth Obs. Geoinformation*, vol. 119, p. 103330, 2023, doi: 10.1016/j.jag.2023.103330.

[2] M. Z. Hesari, S. Shataee, Y. Maghsoudi, J. Mohammadi, J. E. S. Fransson, and H. J. Persson, "Forest Variable Estimations Using TanDEM-X Data in Hyrcanian Forests," *Can. J. Remote Sens.*, pp. 1–11, 2020, doi: 10.1080/07038992.2020.1763790.

[3] T. H. Tarekegn, A. T. Haile, T. Rientjes, P. Reggiani, and D. Alkema, "Assessment of an ASTER-generated DEM for 2D hydrodynamic flood modeling," *Int. J. Appl. Earth Obs. Geoinformation*, vol. 12, no. 6, pp. 457–465, 2010, doi: 10.1016/j.jag.2010.05.007.

[4] D. Yamazaki, T. Sato, S. Kanae, Y. Hirabayashi, and P. D. Bates, "Regional flood dynamics in a bifurcating mega delta simulated in a global river model," *Geophys. Res. Lett.*, vol. 41, no. 9, pp. 3127–3135, 2014, doi: 10.1002/2014GL059744.

[5] Y. J. Su and Q. H. Guo, "A practical method for SRTM DEM correction over vegetated mountain areas," *ISPRS J. Photogramm. Remote Sens.*, vol. 87, pp. 216–228, 2014, doi: 10.1016/j.isprsjprs.2013.11.009.

[6] M. J. Soja, H. Persson, and L. Ulander, "Estimation of Forest Height and Canopy Density From a Single InSAR Correlation Coefficient," *IEEE Geosci. Remote Sens. Lett.*, vol. 12, no. 3, pp. 646–650, 2015, doi: 10.1109/LGRS.2014.2354551.

[7] R. N. Treuhaft, S. N. Madsen, M. Moghaddam, and J. J. Van Zyl, "Vegetation characteristics and underlying topography from interferometric radar," *Radio Sci.*, vol. 31, no. 6, pp. 1449–1485, 1996, doi: 10.1029/96RS01763.

[8] I. Hajnsek, F. Kugler, S. K. Lee, and K. P. Papathanassiou, "Tropical-Forest-Parameter Estimation by Means of Pol-InSAR: The INDREX-II Campaign," *IEEE Trans. Geosci. Remote Sens.*, vol. 47, no. 2, pp. 481–493, 2009, doi: 10.1109/TGRS.2008.2009437.

[9] S. Hosseini and F. Garestier, "Pol-InSAR sensitivity to hemi-boreal forest structure at L-and P-bands," *Int. J. Appl. Earth Obs. Geoinformation*, vol. 94, p. 102213, 2021, doi: 10.1016/j.jag.2020.102213.

[10] H. Q. Fu, J. J. Zhu, C. C. Wang, R. Zhao, and Q. H. Xie, "Underlying Topography Estimation Over Forest Areas Using Single-Baseline InSAR Data," *IEEE Trans. Geosci. Remote Sens.*, vol. 57, no. 5, pp. 2876–2888, 2019, doi: 10.1109/TGRS.2018.2878357.

[11] M. J. Soja and L. M. Ulander, "Mapping topography and forest parameters in a boreal forest with dual-baseline TanDEM-X data and the two-level model," in *Proceedings of EUSAR 2016: 11th European Conference on Synthetic Aperture Radar*, Hamburg, Germany: VDE, 2016, pp. 1–4.

[12] R. N. Treuhaft *et al.*, "Vegetation profiles in tropical forests from multibaseline interferometric synthetic aperture radar, field, and lidar measurements," *J. Geophys. Res. Atmospheres*, vol. 114, no. D23, pp. 1–16, 2009, doi: 10.1029/2008JD011674.

[13] A. Reigber and A. Moreira, "First demonstration of airborne SAR tomography using multibaseline L-band data," *IEEE Trans. Geosci. Remote Sens.*, vol. 38, no. 5, pp. 2142–2152, 2000, doi: 10.1109/36.868873.

[14] M. Pardini, J. S. Kim, K. Papathanassiou, and I. Hajnsek, "Height and 3-D Structure Estimation of African Tropical Forests With Multi-Baseline SAR: Results From the AfriSAR Campaign," in *IEEE International Geoscience and Remote Sensing Symposium*, Fort Worth, TX, USA: IEEE, 2017. doi: 10.1109/IGARSS.2017.8127950.

[15] M. Lavalle, M. Simard, and S. Hensley, "A temporal decorrelation model for polarimetric radar interferometers," *IEEE Trans. Geosci. Remote Sens.*, vol. 50, no. 7, pp. 2880–2888, 2011, doi: 10.1109/TGRS.2011.2174367.

[16] F. Kugler, D. Schulze, I. Hajnsek, H. Pretzsch, and K. P. Papathanassiou, "TanDEM-X Pol-InSAR Performance for Forest Height Estimation," *IEEE Trans. Geosci. Remote Sens.*, vol. 52, no. 10, pp. 6404–6422, 2014, doi: 10.1109/TGRS.2013.2296533.

[17] G. Krieger *et al.*, "TanDEM-X: A Satellite Formation for High-Resolution SAR Interferometry," *IEEE Trans. Geosci. Remote Sens.*, vol. 45, no. 11, pp. 3317–3341, 2007, doi: 10.1109/TGRS.2007.900693.

[18] S. Raveendrakumar, U. Khati, M. Musthafa, G. Singh, and S. Tebaldini, "Use of TanDEM-X PolInSAR for canopy height retrieval over tropical forests in the Western Ghats, India," *Front. For. Glob. Change*, vol. 5, p. 836205, 2022, doi: 10.3389/ffgc.2022.836205.

[19] J. I. Askne, J. E. Fransson, M. Santoro, M. J. Soja, and L. M. Ulander, "Model-based biomass estimation of a hemi-boreal forest from multitemporal TanDEM-X acquisitions," *Remote Sens.*, vol. 5, no. 11, pp. 5574–5597, 2013, doi: 10.3390/rs5115574.

[20] L. W. Kenyi, R. Dubayah, M. Hofton, and M. Schardt, "Comparative analysis of SRTM–NED vegetation canopy height to LIDAR-derived vegetation canopy metrics," *Int. J. Remote Sens.*, vol. 30, no. 11, pp. 2797–2811, 2009, doi: 10.1080/01431160802555853.

[21] M. J. Soja, H. J. Persson, and L. Ulander, "Estimation of Forest Biomass From Two-Level Model Inversion of Single-Pass InSAR Data," *IEEE Trans. Geosci. Remote Sens.*, vol. 53, no. 9, pp. 5083–5099, 2015, doi: 10.1109/TGRS.2015.2417205.

[22] Y. Sadeghi, B. St-Onge, B. Leblon, and M. Simard, "Canopy height model (CHM) derived from a TanDEM-X InSAR DSM and an airborne lidar DTM in boreal forest," *IEEE J. Sel. Top. Appl. Earth Obs. Remote Sens.*, vol. 9, no. 1, pp. 381–397, 2016, doi: 10.1109/JSTARS.2015.2512230.

[23] S. Solberg, R. Astrup, J. Breidenbach, B. Nilsen, and D. Weydahl, "Monitoring spruce volume and biomass with InSAR data from TanDEM-X," *Remote Sens. Environ.*, vol. 139, pp. 60–67, 2013, doi: 10.1016/j.rse.2013.07.036.

[24] H. Chen, S. R. Cloude, and D. G. Goodenough, "Forest Canopy Height Estimation Using Tandem-X Coherence Data," *IEEE J. Sel. Top. Appl. Earth Obs. Remote Sens.*, vol. 9, no. 7, pp. 3177–3188, 2016, doi: 10.1109/JSTARS.2016.2582722.

[25] C. Gómez *et al.*, "Canopy height estimation in Mediterranean forests of Spain with TanDEM-X data," *IEEE J. Sel. Top. Appl. Earth Obs. Remote Sens.*, vol. 14, pp. 2956–2970, 2021, doi: 10.1109/JSTARS.2021.3060691.

[26] A. Olesk, K. Voormansik, A. Vain, M. Noorma, and J. Praks, "Seasonal Differences in Forest Height Estimation From Interferometric TanDEM-X Coherence Data," *IEEE J. Sel. Top. Appl. Earth Obs. Remote Sens.*, vol. 8, no. 12, pp. 5565–5572, 2015, doi: 10.1109/JSTARS.2015.2501648.

[27] L. Zhao, E. Chen, Z. Li, W. Zhang, and Y. Fan, "A new approach for forest height inversion using X-band single-pass InSAR coherence data," *IEEE Trans. Geosci. Remote Sens.*, vol. 60, pp. 1–18, 2021, doi: 10.1109/TGRS.2021.3072125.

[28] R. Guliaev, V. Cazcarra-Bes, M. Pardini, and K. Papathanassiou, "Forest height estimation by means of TanDEM-X InSAR and waveform lidar data," *IEEE J. Sel. Top. Appl. Earth Obs. Remote Sens.*, vol. 14, pp. 3084–3094, 2021, doi: 10.1109/JSTARS.2021.3058837.

[29] C. Choi *et al.*, "Large-Scale Forest Height Mapping by Combining TanDEM-X and GEDI Data," *IEEE J. Sel. Top. Appl. Earth Obs. Remote Sens.*, vol. 16, pp. 2374–2385, 2023, doi: 10.1109/JSTARS.2023.3244866.

[30] Y. Lei, R. Treuhaft, and F. Gonçalves, "Automated estimation of forest height and underlying topography over a Brazilian tropical forest with single-baseline single-polarization TanDEM-X SAR interferometry," *Remote Sens. Environ.*, vol. 252, p. 112132, 2021, doi: 10.1016/j.rse.2020.112132.

[31] H. Q. Wang *et al.*, "Estimation of subcanopy topography based on single-baseline TanDEM-X InSAR data," *J. Geod.*, vol. 95, no. 7, pp. 1–19, 2021, doi: 10.1007/s00190-021-01519-3.

[32] J. Dall, "InSAR Elevation Bias Caused by Penetration Into Uniform Volumes," *IEEE Trans. Geosci. Remote Sens.*, vol. 45, no. 7, pp. 2319–2324, 2007, doi: 10.1109/TGRS.2007.896613.

[33] H. Q. Fu, J. J. Zhu, C. C. Wang, R. Zhao, and Q. H. Xie, "Atmospheric Effect Correction for InSAR With Wavelet Decomposition-Based Correlation Analysis Between Multipolarization Interferograms," *IEEE Trans. Geosci. Remote Sens.*, vol. 56, no. 10, pp. 5614–5625, 2018, doi: 10.1109/TGRS.2018.2821716.

[34] R. F. Hanssen, *Radar Interferometry Data Interpretation and Error Analysis*. Springer, 2001.

[35] Z. Liu, C. Zhou, H. Fu, J. Zhu, and T. Zuo, "A framework for correcting ionospheric artifacts and atmospheric effects to generate high accuracy InSAR DEM," *Remote Sens.*, vol. 12, no. 2, p. 318, 2020.

[36] H. A. Zebker and J. Villasenor, "Decorrelation in interferometric radar echoes," *IEEE Trans. Geosci. Remote Sens.*, vol. 30, no. 5, pp. 950–959, 1992, doi: 10.1109/36.175330.

[37] M. Martone, B. Bräutigam, P. Rizzoli, C. Gonzalez, M. Bachmann, and G. Krieger, "Coherence evaluation of TanDEM-X interferometric data," *ISPRS J. Photogramm. Remote Sens.*, vol. 73, pp. 21–29, 2012, doi: 10.1016/j.isprsjprs.2012.06.006.

[38] S. R. Cloude and K. P. Papathanassiou, "Polarimetric SAR Interferometry," *IEEE Trans. Geosci. Remote Sens.*, vol. 36, no. 5, pp. 1551–1565, 1998, doi: 10.1109/36.718859.

[39] S. R. Cloude, *Polarisation: Applications in Remote Sensing*. London, U.K.: Oxford Univ. Press, 2009.

[40] K. P. Papathanassiou and S. R. Cloude, "Single-baseline polarimetric SAR interferometry," *IEEE Trans. Geosci. Remote Sens.*, vol. 39, no. 11, pp. 2352–2363, 2001, doi: 10.1109/36.964971.

[41] J. Praks, O. Antropov, and M. T. Hallikainen, "LIDAR-Aided SAR Interferometry Studies in Boreal Forest: Scattering Phase Center and Extinction Coefficient at X- and L-Band," *IEEE Trans. Geosci. Remote Sens.*, vol. 50, no. 10, pp. 3831–3843, 2012, doi: 10.1109/TGRS.2012.2185803.

[42] H. Q. Wang, J. J. Zhu, H. Q. Fu, G. C. Feng, and C. C. Wang, "Modeling and Robust Estimation for the Residual Motion Error in Airborne SAR Interferometry," *IEEE Geosci. Remote Sens. Lett.*, vol. 16, no. 1, pp. 1–5, 2018, doi: 10.1109/LGRS.2018.2867868.

[43] R. M. Goldstein and C. L. Werner, "Radar interferogram filtering for geophysical applications," *Geophys. Res. Lett.*, vol. 25, no. 21, pp. 4035–4038, 1998, doi: 10.1029/1998GL900033.

[44] M. Costantini, "A novel phase unwrapping method based on network programming," *IEEE Trans. Geosci. Remote Sens.*, vol. 36, no. 3, pp. 813–821, 1998, doi: 10.1109/36.673674.

[45] B. Xu, Z. Li, Q. Wang, M. Jiang, J. Zhu, and X. Ding, "A refined strategy for removing composite errors of SAR interferogram," *IEEE Geosci. Remote Sens. Lett.*, vol. 11, no. 1, pp. 143–147, 2013, doi: 10.1109/LGRS.2013.2250903.

[46] H. Laudon, I. Taberman, A. Ågren, M. Futter, M. Ottosson-Löfvenius, and K. Bishop, "The Krycklan Catchment Study—A flagship infrastructure for hydrology, biogeochemistry, and climate research in the boreal landscape," *Water Resour. Res.*, vol. 49, no. 10, pp. 7154–7158, 2013, doi: 10.1002/wrcr.20520.

[47] A. T. Caicoya, F. Kugler, I. Hajnsek, and K. P. Papathanassiou, "Large-scale biomass classification in boreal forests with TanDEM-X data," *IEEE Trans. Geosci. Remote Sens.*, vol. 54, no. 10, pp. 5935–5951, 2016, doi: 10.1109/TGRS.2016.2575542.

[48] T. Markus *et al.*, "The Ice, Cloud, and land Elevation Satellite-2 (ICESat-2): science requirements, concept, and implementation," *Remote Sens. Environ.*, vol. 190, pp. 260–273, 2017, doi: 10.1016/j.rse.2016.12.029.

[49] A. Neuenschwander and K. Pitts, "The ATL08 land and vegetation product for the ICESat-2 Mission," *Remote Sens. Environ.*, vol. 221, pp. 247–259, 2019, doi: 10.1016/j.rse.2018.11.005.

[50] I. Hajnsek *et al.*, "BIOSAR 2008 Technical Assistance for the Development of Airborne SAR and Geophysical Measurements during the BioSAR 2008 Experiment, Final Report," ESA contract No. 22052/08/NL/CT, 2008. [Online]. Available: https://earth.esa.int/c/document_library/get_file?folderId=21020&name= DLFE-21903.pdf.

[51] L. M. H. Ulander *et al.*, "BioSAR 2010. Technical Assistance for the Development of Airborne SAR and Geophysical Measurements during the BioSAR 2010 Experiment: Final Report," European Space Agency: Noordwijk, The Netherlands, ESA Contract No. 4000102285/10/NL/JA/ef, 2010.

[52] A. A. Villar *et al.*, "Spanish national plan for territory observation (PNOT)," in *The International Archives of the Photogrammetry, Remote Sensing and Spatial Information Sciences*, Beijing, China, 2008, pp. 1729–1733.

[53] T. Fatoyinbo *et al.*, "The NASA AfriSAR campaign: Airborne SAR and lidar measurements of tropical forest structure and biomass in support of current and future space missions," *Remote Sens. Environ.*, vol. 264, p. 112533, 2021, doi: 10.1016/j.rse.2021.112533.

[54] A. Gruber, B. Wessel, M. Huber, and A. Roth, "Operational TanDEM-X DEM calibration and first validation results," *ISPRS J. Photogramm. Remote Sens.*, vol. 73, pp. 39–49, 2012, doi: 10.1016/j.isprsjprs.2012.06.002.

[55] H. Q. Fu, J. J. Zhu, C. C. Wang, and Z. W. Li, "Underlying topography extraction over forest areas from multi-baseline PolInSAR data," *J. Geod.*, vol. 92, no. 7, pp. 727–741, 2018.

[56] J. I. Askne, M. J. Soja, and L. M. Ulander, "Biomass estimation in a boreal forest from TanDEM-X data, lidar DTM, and the interferometric water cloud model," *Remote Sens. Environ.*, vol. 196, pp. 265–278, 2017, doi: 10.1016/j.rse.2017.05.010.

[57] A. Olesk, J. Praks, O. Antropov, K. Zalite, T. Arumäe, and K. Voormansik, "Interferometric SAR coherence models for characterization of hemiboreal forests using TanDEM-X data," *Remote Sens.*, vol. 8, no. 9, p. 700, 2016, doi: 10.3390/rs8090700.

[58] H. Chen, S. R. Cloude, D. G. Goodenough, D. A. Hill, and A. Nesdoly, "Radar Forest Height Estimation in Mountainous Terrain Using Tandem-X Coherence Data," *IEEE J. Sel. Top. Appl. Earth Obs. Remote Sens.*, vol. 11, no. 10, pp. 1–10, 2018, doi: 10.1109/JSTARS.2018.2866059.

[59] C. Xing, H. Wang, Z. Zhang, J. Yin, and J. Yang, "A Review of Forest Height Inversion by PolInSAR: Theory, Advances, and Perspectives," *Remote Sens.*, vol. 15, no. 15, p. 3781, 2023, doi: 10.3390/rs15153781.

[60] S.-K. Lee, T. E. Fatoyinbo, D. Lagomasino, E. Feliciano, and C. Trettin, "Multibaseline tandem-x mangrove height estimation: The selection of the vertical wavenumber," *IEEE J. Sel. Top. Appl. Earth Obs. Remote Sens.*, vol. 11, no. 10, pp. 3434–3442, 2018, doi: 10.1109/JSTARS.2018.2835647.

[61] R. Deo, C. Rossi, M. Eineder, T. Fritz, and Y. S. Rao, "Framework for Fusion of Ascending and Descending Pass TanDEM-X Raw DEMs," *IEEE J. Sel. Top. Appl. Earth Obs. Remote Sens.*, vol. 8, no. 7, pp. 3347–3355, 2015, doi: 10.1109/JSTARS.2015.2431433.

Zhiwei Liu received the bachelor's degree in surveying and mapping engineering from Changchun Institute of Technology, Changchun, China, in 2015, and the master's degrees in geodesy and survey engineering, in 2019, from Central South University, Changsha, China, where he is currently working toward the Ph.D. degree in geodesy and surveying engineering. His research interests include SAR/InSAR/PolInSAR data processing, and the applications for forest phenology monitoring and sub-canopy topography inversion. Now he is also a joint Ph.D. student with the University of Alicante, Alicante, Spain.

Jianjun Zhu received the M.Eng. degree in engineering surveying and the Ph.D. degree in geodesy and surveying engineering from the Central South University of Technology (now Central South University), Changsha, China, in 1985 and 1998, respectively. From 1998 to 1999, he was a Research Assistant with the Department of Land Surveying and Geo-informatics, The Hong Kong Polytechnic University, Hong Kong. From 2000 to 2001, he was a Post-Doctoral Fellow with the Center for Research on Geomatics, Laval University, Québec City, Canada.

He is currently a Full Professor with the School of Geosciences and Info-Physics, Central South University. His research interests include the theory of errors and surveying adjustment and its applications in interferometric satellite synthetic aperture radar.

Juan M. Lopez-Sanchez (Senior Member, IEEE) received the Ingeniero (M.S.) and Doctor Ingeniero (Ph.D.) degrees in telecommunication engineering from the Technical University of Valencia, Vsalencia, Spain, in 1996 and 2000, respectively.

From 1998 to 1999, he was a Predoctoral Grantholder with the Space Applications Institute, Joint Research Centre of the European Commission, Ispra, Italy. Since 2000, he has been leading the Signals, Systems and Telecommunication Group, University of Alicante, Alicante, Spain, where he has been a Full Professor since November 2011. His research interests include microwave remote sensing for inversion of biophysical parameters, polarimetric and interferometric techniques, SAR imaging algorithms, and applications of radar remote sensing in agriculture and geophysics.

Dr. Lopez-Sanchez was the recipient of the Indra Award for the Best Ph.D. Thesis about radar in Spain in 2001. From 2006 to 2012, he was the Chair of the Spanish Chapter of the IEEE Geoscience and Remote Sensing Society. He has coauthored more than 100 papers in refereed journals and more than 150 papers and presentations in international conferences and symposia.

Cristina Gómez received the M.Sc. degree in applied geospatial technologies from the University of Aberdeen, Aberdeen, U.K., in 2006, and the Ph.D. degree in conservation and sustainable use of forest systems from the University of Valladolid, Valladolid, Spain, in 2014.

She is an M.Sc. Forest Engineer at the Technical University of Madrid, Madrid, Spain, in 2001. Her current research focuses on the characterization and monitoring of environmental dynamics at different spatio–temporal scales, integrating a range of geospatial technologies. She employs time-series analysis of remotely sensed data for assessment of forest processes of change, like drastic and subtle disturbance, or natural succession including regeneration, growth, decline, and mortality. She is particularly interested in forest phenological traits and variations through time, as well as long-term trends of change to help assessing forest structure and ecosystemic services.

Haiqiang Fu (Senior Member, IEEE) received the bachelors' degree in remote sensing science and technology from Southwest Jiaotong University, Chengdu, China, in 2011. And he has the master's degree and the Ph.D. degree in geodesy and survey engineering from Central South University, Changsha, China, in 2014 and 2018, respectively.

He is currently an Associate Professor with the School of Geosciences and Info-Physics, Central South University. His research interests include polarimetric SAR interferometry and its applications for monitoring forest parameters and extracting the underlying topography over forest areas.

Cui Zhou was born in Shaoyang, Hunan, China, in 1982. She received the B.Eng. degree in computer and M.Agr. degree in information engineering from Central South University of Forestry and Technology, China, in 2005 and 2010, respectively, and the Ph.D. degree in surveying science and technology from Central South University, China, in 2015.

Since 2005, she has been at Central South University of Forestry and Technology, where she is currently a professor in geography. Her current research and interest areas include remote sensing, data fusion, terrain modelling and analysis.

Prof. Zhou awards and honors include outstanding talent in Hunan Province, China and ents scholars in Central South University of Forestry and Technology.

Huiqiang Wang received the bachelor's degree in surveying engineering from the University of Science and Technology Liaoning, Anshan, China, in 2013, and the masters' degree and Ph.D. degree in geodesy and survey engineering from Central South University, Changsha, China, in 2016 and 2021. His research interests include SAR interferometry (InSAR) and polarimetric SAR interferometry (PolInSAR) data processing, and the applications for monitoring the ground deformation and extracting the sub-canopy topography over forest areas.

Rong Zhao received the Bachelor's degree in surveying engineering from Henan University of Urban Construction, Henan, China, in 2011. And she received a Master's degree and Ph. D degree in photogrammetry and remote sensing from Central South University, Changsha, China, in 2014 and 2020, respectively.

She is currently an associate professor in the College of Advanced Interdisciplinary Studies, Central South University of Forestry and Technology, Changsha, China. Her research interests include Interferometric Synthetic Aperture Radar (InSAR), polarimetric SAR interferometry (PolInSAR), space-borne LiDAR data processing, and its applications for monitoring surface deformation, forest parameters and extracting the related physical parameters.